Dynamical Modeling and Numerical Methods for CAR-T Cell Therapy and Viral Tweets

Trevor Crupi

A thesis

submitted in partial fulfillment of the

requirements for the degree of

Master of Science

University of Washington
2022

Committee:
Ivana Bozic
Amin Rahman
Nathan Kutz

Program Authorized to Offer Degree:
Applied Mathematics

University of Washington

Abstract

Dynamical Modeling and Numerical Methods for CAR-T Cell Therapy and Viral Tweets

Trevor Crupi

Co-chairs of the Supervisory Committee:

Assistant Professor Ivana Bozic
Applied Mathematics

Acting Instructor Amin Rahman
Applied Mathematics

The development of CAR-T cell immunotherapies has been one of the most exciting advancements in the field of cancer research over the last decade. Many mathematical models have been proposed to better understand the nonlinear dynamics between immune cells and tumor cells. In this thesis, we introduce a system of partial differential equations to model CAR-T cell therapies for 3-dimensional tumors. We then numerically approximate this system using the finite element method for 3 different cases: purely diffusive tumor growth, tumor growth with logistic forcing, and the coupled CAR-T cell system. We show that mixed finite elements for the coupled system has the potential to elucidate the behavior of CAR-T cell immunotherapies on complex tumor geometries.

Misinformation has become pervasive throughout modern society, playing a major role in recent democratic elections and the ongoing COVID-19 pandemic. Understanding the way viral content spreads on the internet will help shed light on methods that can prevent misinformation spread. Thus, we formulate a discrete dynamical system to model retweet cascades on Twitter. We utilize extreme value theory as a framework to determine superusers in a retweet cascade, and re-forecast our dynamical system to account for them. We show that re-forecasting for superusers yields extremely high accuracy across the most viral tweets in our dataset.

Acknowledgements

I would like to thank my advisors, Dr. Amin Rahman and Dr. Ivana Bozic, for encouraging me to explore these topics and guiding me throughout the process. I'd also like to thank my family for constantly encouraging me to pursue what I love. Finally, I'd like to thank the University of Washington Applied Mathematics Department for giving me the opportunity to research and learn in an exceptional environment with incredible classmates and professors.

DEDICATION

To my family.

Contents

Chapter 1

Finite Element Methods for Spatio-Temporal CAR T-Cell Models

1.1 Introduction

The development of CAR-T cell immunotherapies has been one of the most exciting advancements in the field of cancer research over the last decade. CAR-T cells are immune cells that have been genetically modified with chimeric antigen receptor (CAR), a synthetic receptor that redirects immune cells to destroy other cells expressing specific antigens [44]. Since 2017, the FDA has approved 6 different types of CAR-T cell therapies. All therapies with FDA approval have been for liquid tumors, such as lymphoma, leukemia, and multiple myeloma. While the process has shown incredible promise for liquid tumors, the treatment still remains shaky for solid tumors [33], [44]. In addition, there are still some questions around efficacy. A 2020 study by Sermer et al. found that CAR-T cell therapy led to long term survival in less than half of patients treated for diffuse large B-cell lymphoma [42]. Thus, more work needs to be done to understand the efficacy and long term effects of CAR-T cell therapies.

One way to approach this is through mathematical modeling. Several mathematical methods have been proposed to model immune cell interactions, immunotherapies, and CAR-T cell therapies to get a better understanding of the dynamics underlying the complex biological interactions between tumor cells, immune cells, and CAR-T cells. Kuznetsov et al. in [22] proposed a 2-dimensional, non-spatial system of ordinary

differential equations that modeled the nonlinear interaction between tumor cells and immune cells. Several new models built on top of the this one by adding new equations or biological assumptions. Similar models include the work of Kirschner and Panetta [21], Dong et al. [12], and Moore and Li [34]. Specifically for CAR-T cells, Hopkins et al. [15] proposed a method to investigate the side effect of cytokine release syndrome (CRS) in CAR-T cell patients. Hardiansyah and Ng used a quantitative systems pharmacology approach to understand the connection between CAR-T cell dosage size and CRS [14]. Owens and Bozic utilized a 4-dimensional system of ordinary differential equations to model CAR-T cell therapies in connection with patient preconditioning plans [37].

In this chapter, we introduce a system of partial differential equations (PDEs) to model CAR-T cell therapies for 3-dimensional tumors. We use a finite element approach to solve this PDE system over a unit cube mesh for 3 different cases: purely diffusive tumor growth, tumor growth with logistic forcing, and finally we use mixed finite element methods to solve the full system of coupled equations. This approach shows that spatio-temporal models for cancer have the potential to elucidate the behavior of immunotherapies, and that the finite element method is a good numerical approximation technique to capture the behavior of these models on more complicated domains.

1.2 Deterministic Models

1.2.1 Tumor Growth Models

The simplest deterministic models for tumor growth are based on population biology. These models typically aim to measure the number of tumor cells as a function of time using an ordinary differential equation (ODE) model. Let the total number of tumor cells at a given time t be denoted $N(t)$ and assume that all tumor cells divide at a certain rate r. From this simple assumption, we can create our first ODE model:

$$\frac{dN(t)}{dt} = rN(t).$$

This equation is interpreted as saying that the rate of change in the total number of tumor cells is equal to the current number of tumor cells multiplied by the rate at which those cells will divide. If we assume we start

with 1 tumor cell as the result of a genetic mutation, i.e., $N(0) = 1$, we can solve this equation directly:

$$N(t) = e^{rt}.$$

In other words, the tumor cells grow exponentially. Fig. 1.1 shows the solution of this equation for $r = 0.1$ and 0.25. In practical applications, we compare biological data to our equations in order to determine the growth rate.

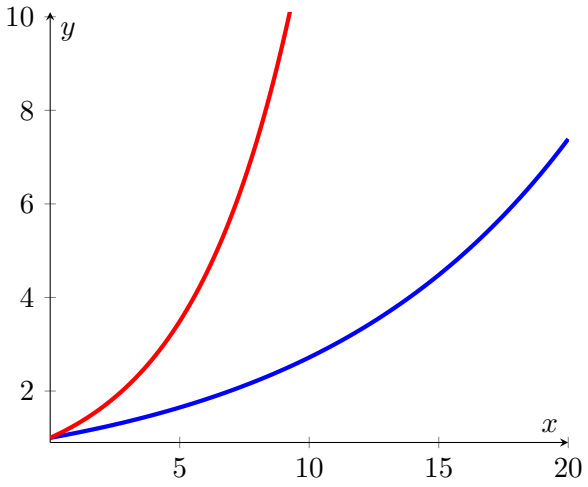

Figure 1.1: The graph of e^{rx} with $r = 0.1$ (blue), $r = 0.25$ (red).

If a tumor grows large enough, it reaches a point where tumor cells must compete for resources. Since some tumor cells aren't able to get the resources they need, they die off. When the tumor reaches this size, we say it has reached its *carrying capacity*, denoted by K. In population dynamics, this is typically modeled using the Verhulst equation [49]:

$$\frac{dN(t)}{dt} = rN(t)\left(1 - \frac{N(t)}{K}\right).$$

We see that this is equivalent to the exponential equation with an additional $1 - \frac{N(t)}{K}$ term. Since $N(t) \leq K \implies \frac{N(t)}{K} \leq 1$, we see that $1 - \frac{N(t)}{K} \to 0$ as $N(t) \to K$. Thus, this additional term accounts for the gradual slowing of the growth rate as the number of cells approaches the carrying capacity. Using the initial

condition $N(0) = 1$, this equation has the solution:

$$N(t) = \frac{Ke^{rt}}{K + e^{rt} - 1}.$$

A couple solutions to the Verhulst equation for different values of r are plotted in Fig. 1.2 using a carrying capacity of 100.

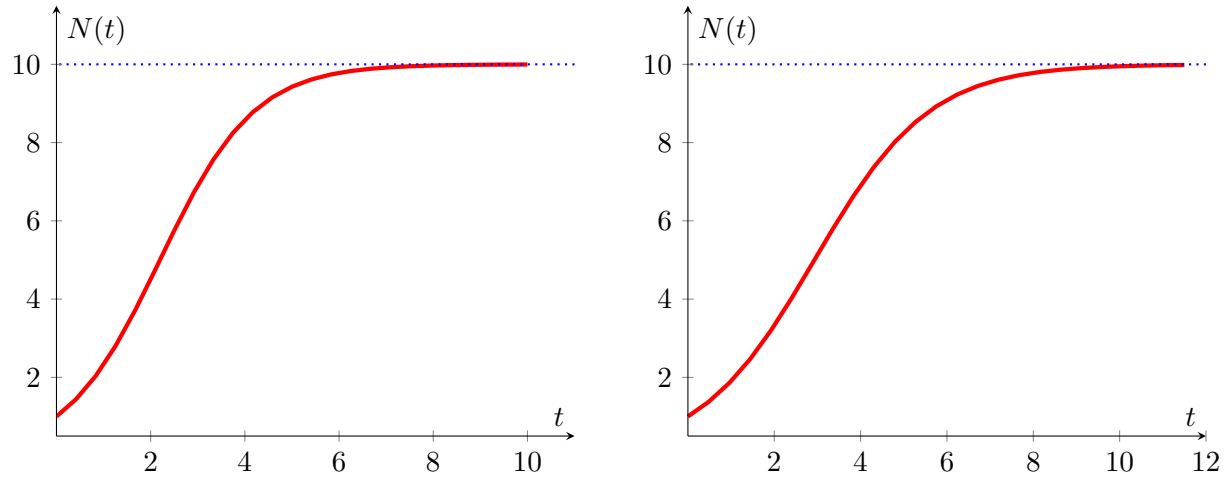

Figure 1.2: The solution to the Verhulst equation with $r = 1$ (left), $r = 0.75$ (right).

More advanced 1-dimensional tumor growth ODE models can be realized by introducing cell death, drug dosage, and other biological phenomenon. We can also introduce systems of ordinary differential equations to model different populations of cancer cells that are coupled together. For instance, we can consider a two cell population with drug sensitive and drug resistant cells. This is similar to the model studied by Tomasetti in [46]. As mentioned in the biological background, drug sensitive tumor cells have the capacity to mutate and become resistant to certain treatments. Here we consider sensitive cells $S(t)$ which divide at a rate b_S and die at a rate d_S, and resistant cells $R(t)$ which divide at a rate b_R and die at a rate d_R. We also allow sensitive cells to mutate into resistant cells at a rate u. We can write this as a system of two coupled ODEs.

$$\begin{aligned}
\frac{dS}{dt} &= bS(t) - dS(t) - uS(t), \\
\frac{dR}{dt} &= b_R R(t) - d_R R(t) + buS(t).
\end{aligned}$$

Using $S(0) = 1$ and $R(0) = 0$, these equations have the analytical solution

$$S(t) = e^{(b(1-u)-d)t},$$
$$R(t) = bu\frac{e^{(b_R-d_R)t} - e^{(b(1-u)-d)t}}{(b_R - d_R) - (b(1-u) - d)}.$$

The solution to these equations has different trajectories for $\Delta < 1$, $\Delta > 1$, and $\Delta = 1$, where

$$\Delta = \frac{b_R - d_R}{b - d}.$$

These cases are called deleterious, advantageous, and neutral respectively, and the different cases correspond to different tumor growth scenarios, showing how even a simple model can give useful insight into the dynamics of tumor growth.

1.2.2 CAR-T cell Models

We now formulate an ODE model to describe CAR-T cells in patients. This model was analyzed by Owens and Bozic in [36]. We let $T(t)$ be the tumor cell count and $E(t)$ be the endogenous effector cell count. By endogenous effector cell, we mean both endogenous and engineered immune cells (CAR-T cells). We can write the following system of coupled ODEs

$$\frac{dT}{dt} = aT(1 - bT) - D_E, \tag{1.1}$$
$$\frac{dE}{dt} = g - m_E E + j_E \frac{D_E^2}{k + D_E^2} E - q_E ET, \tag{1.2}$$

where

$$D_E = d_E \frac{\left(\frac{E}{T}\right)^l}{s + \left(\frac{E}{T}\right)^l} T.$$

Is the *tumor cell lysis rate*, a non-linear coupling term. This defines the coupled dynamics between the endogenous effector cells and the tumor cells. Table 1.1 describes each of the parameters in our system. When $E = 0$, $D_E = 0$ and thus equation 1.1 becomes a logistic (Verhulst) equation with carrying capacity b^{-1}.

Parameter List for Owens and Bozic Models in [36], [37]		
Parameter	Description	Units
a	Tumor Cell Count Growth Rate	day^{-1}
b^{-1}	Carrying capacity of the tumor	cells
d_E	Saturation level of fractional tumor kill by effector cells	day^{-1}
d_C	Saturation level of fractional tumor kill by CAR-T cells	day^{-1}
g	Base recruitment rate of effector cells	$\frac{\text{cells}}{\text{day}}$
j	Max recruitment rate of effector cells by tumor lysis	day^{-1}
k	Steepness of effect cell recruitment curve	$\frac{\text{cells}^2}{\text{day}^2}$
l	Exponent of fractional tumor cell kill by effect cells	No units
m_E	Death rate of effector cells	day^{-1}
q_C	Inactivation of CAR-T cells by tumor	$\frac{\text{cells}}{\text{day}}$
m_C	Death rate of CAR-T cells	day^{-1}
q_E	Inactivation of effect cells by tumor	$\frac{\text{cells}}{\text{day}}$
s	Steepness of fractional tumor cell kill by effector cells	No units

Table 1.1: Parameter list for the ODE model in [36],[37]

We can non-dimensionalize this system by allowing $x(t) = bT$, $y(t) = \frac{aE}{g}$, $D^* = \frac{D}{a}$, $t^* = at$, and $s_* = s\left(\frac{a}{gb}\right)^l$. After non-dimensionalizing we obtain:

$$\begin{aligned}
\frac{dx}{dt} &= x(1 - D_* - x),\\
\frac{dy}{dt} &= 1 + y\left(j_*\frac{D_*^2x^2}{k_* + D_*^2x^2} - q_*x - m_*\right),\\
D_* &= d_*\frac{\left(\frac{y}{x}\right)^l}{s_* + \left(\frac{y}{x}\right)^l},
\end{aligned}$$

where $d_* = \frac{d}{a}$, $j_* = \frac{j}{a}$, $k_* = \frac{b^2k}{a^2}$, $m_* = \frac{m}{a}$, and $q_* = \frac{q}{ab}$. For simplicity we drop the stars from the

non-dimensional equations. Our final non-dimensional system is given by

$$\frac{dx}{dt} = x(1 - D - x), \tag{1.3}$$

$$\frac{dy}{dt} = 1 + y\left(j\frac{D^2x^2}{k + D^2x^2} - qx - m\right), \tag{1.4}$$

with $D = d\frac{\left(\frac{y}{x}\right)^l}{s+\left(\frac{y}{x}\right)^l}$. In the same paper, Owens and Bozic introduced an ODE system to model tumor growth with chemotherapy treatment. They introduced a new variable $C(t)$ based on the method of de Pillis et al [11] representing the concentration of a chemotherapy drug at time t. The dimensionalized system is given by

$$\frac{dT}{dt} = aT(1 - bT) - D_E - K_T(1 - e^{-C})T, \tag{1.5}$$

$$\frac{dE}{dt} = g - m_E E + j_E\frac{D_E^2}{k + D_E^2}E - q_E ET - K_E(1 - e^{-C})E + v_E(t), \tag{1.6}$$

$$\frac{dC}{dt} = -\gamma C + v_C(t). \tag{1.7}$$

Here $K_T(1 - e^{-C})T$ and $K_E(1 - e^{-C})E$ are killing terms that represent the number of tumor and immune cells being killed off by chemotherapy and γ is the decay rate of chemotherapy. $v_C(t)$ is a time-dependent forcing quantity that determines how strong the dose of a chemotherapy drug is at time t

$$v_C(t) = \begin{cases} 0 & \text{if } t \notin \text{ injection times} \\ S & \text{if } t \in \text{ injection times} , \end{cases}$$

where S is the dose strength. Similarly, the CAR-T cells have a time-dependent forcing function, $v_E(t)$, that provides the tumor with a dose level P of CAR-T cells at injection time and 0 otherwise

$$v_E(t) = \begin{cases} 0 & \text{if } t \neq \text{ injection time} \\ P & \text{if } t = \text{ injection times} . \end{cases}$$

Owen's and Bozic use the system 1.7 to plot different possibilities for tumor growth with treatment. Fig. 1.3 is taken from the Owens and Bozic paper [36] and shows different trajectories of the ODE model using

different chemotherapy and CAR-T Cell treatment parameters.

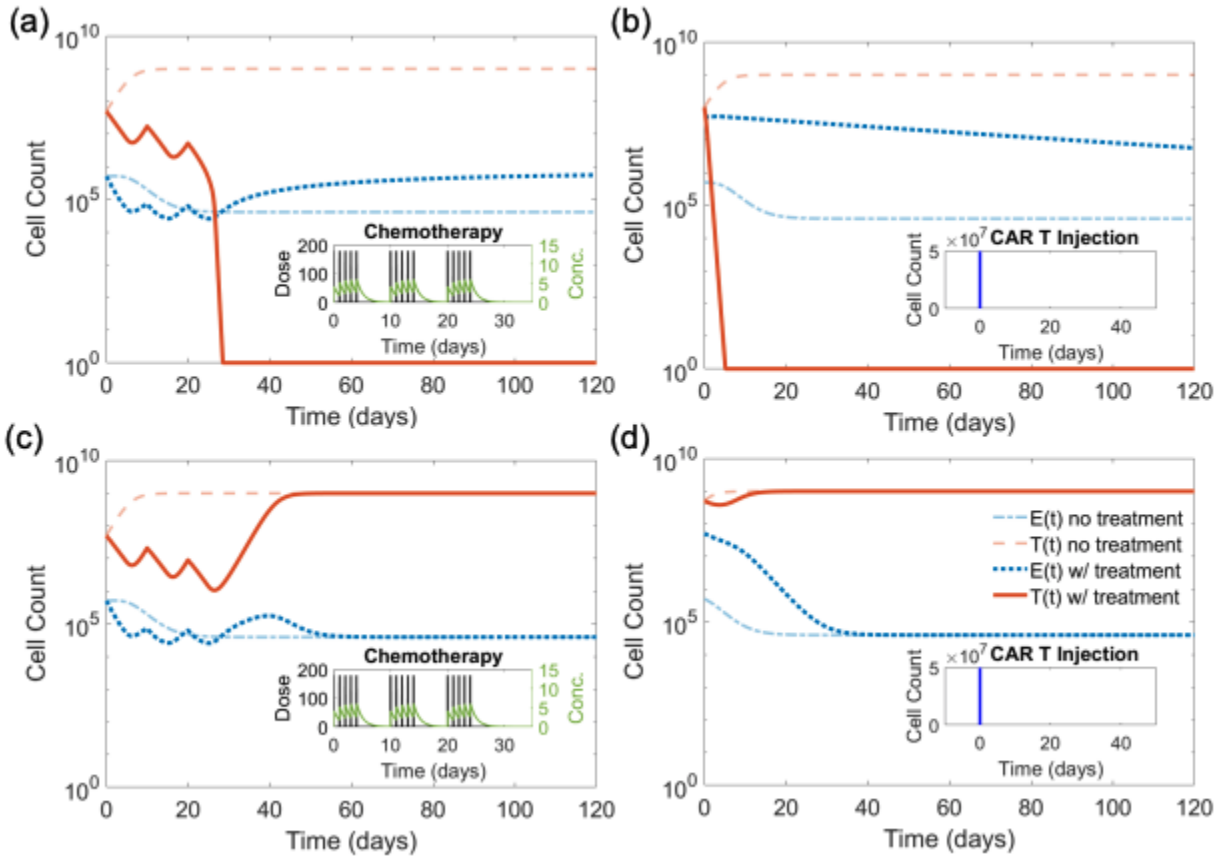

Figure 1.3: Figure originally from [36]. (**a**). Simulation for $T_0 = 5 \times 10^7$ cells, $E_0 = 5 \times 10^5$ cells, showing successful chemotherapy as the number of tumor cells decreases to 0. The dotted lines show the trajectories without treatment. (**b**). Simulation for $T_0 = 1 \times 10^8$ cells, $E_0 = 5 \times 10^5$ cells, showing successful chemotherapy for the same patient parameters from a. The dotted lines shows the trajectories without treatment. (**c**). Simulation using different patient parameters taken from clinical data. We see that even with chemotherapy the patient moves toward the unhealthy outcome despite initially seeing a decrease in the number of tumor cells. The dotted lines show the outcome without treatment. (**d**). The same patient parameters as a and b but using an initial condition of $T_0 = 5 \times 10^8$ cells and $E_0 = 5 \times 10^5$ cells results in an unhealthy outcome.

In [37], Owens and Bozic introduced a slightly refined model using $T(t)$ as the number of tumor cells, $E(t)$ as the number of endogenous effector cells, $C(t)$ the number of CAR-T cells, and $M(t)$ the concentration of the chemotherapy drug. They introduced the ODE system

$$\frac{dT}{dt} = aT(1 - bT) - D_E - D_C - K_T(1 - e^{-M})T, \tag{1.8}$$

$$\frac{dE}{dt} = g - m_E E - j_E \ln\left(\frac{E+C}{K}\right)\frac{D_E^2}{k+D_E^2}E - q_E ET - K_E(1-e^{-M})E, \tag{1.9}$$

$$\frac{dC}{dt} = g - m_C C - j_C \ln\left(\frac{E+C}{K}\right)\frac{D_C^2}{k+D_C^2}C - q_C ET - K_C(1-e^{-M})C, \tag{1.10}$$

$$\frac{dM}{dt} = -\gamma M + v_M(t). \tag{1.11}$$

This model is analogous to the system 1.7 except for the endogenous immune cells and CAR-T cells are split into 2 similar equations. The justification for this is that CAR-T cells are genetically engineered and thus have different parameter values from the endogenous immune cells. The authors performed a dynamical systems analysis and were able to relate the parameters and trajectories of the system to different therapy outcomes. These CAR-T cell ODE models show the validity of a mathematical approach to understand the effects of CAR-T cell therapy on patients. Using a system of ODEs, we can gain an insight into what features of the tumor most influence growth and use these insights to guide cancer therapies. These ODE models will also guide the derivation of spatio-temporal models for cancer treatment.

1.3 Spatio-Temporal Cancer Models

The Owens and Bozic CAR-T cell model shows that useful insights for cancer treatment can be derived from ODE models. ODEs, however, tend to average out population-wide spatial effects, and in an environment such as a tumor, where geometries can often vary widely from patient to patient, this side effect of ODE models can ignore vital spatial features. In order to introduce more precise spatial properties into our system, we make use of partial differential equations (PDEs).

1.3.1 Reaction-Diffusion Equation

Imagine an abstract 3-dimensional tumor Ω which is simply-connected and compact. We define $u(x,t)$ to be the density of tumor cells at a point $x \in \mathbb{R}^3$ at a time $t \in [0,\infty)$. We also define the flux of cells across $\partial\Omega$ as $\phi(x,t)$. The goal is to write a PDE to describe how the tumor concentration changes in time after we inject cells into the tumor Ω. We assume that the tumor Ω exhibits the property of *chemotaxis*, that is, cells

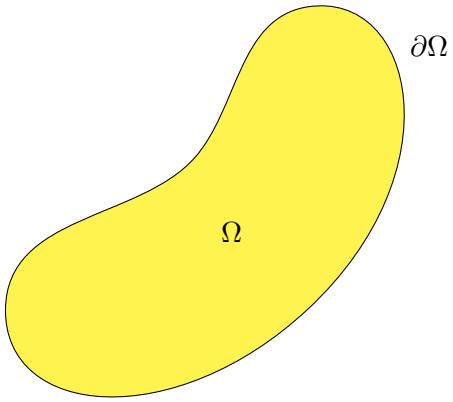

Figure 1.4: Abstract Tumor Ω

flow from areas of high concentration to low concentration. Mathematically, this is written

$$\phi \propto \nabla u \implies \phi = -D(x,t)\nabla u.$$

Here $D(x,t)$ is the *diffusion coefficient* which we've written as a function to show that diffusion varies across the tumor. In order to write this as a PDE, we require a conservation law. Since tumor cells are proliferating and more cells are flowing in across the boundary, we can write the rate of change of the tumor cell density as follows.

Rate of change of tumor cell density = Diffusion of cells (motility) Ω + net cell proliferation Ω.

Using volume integrals, we write this as

$$\frac{d}{dt}\left(\iiint_\Omega u d\Omega\right) = -\oiint_\Omega \phi \cdot \vec{n} d\Omega - \iiint_\Omega F(x,t) d\Omega,$$

and by divergence theorem, we have

$$-\oiint_\Omega \phi \cdot \vec{n} d\Omega = \iiint_\Omega \nabla \cdot (D(x,t)\nabla u) d\Omega.$$

Substituting this into the conservation law:

$$\frac{d}{dt}\left(\iiint_{\Omega} u d\Omega\right) = \iiint_{\Omega} \nabla \cdot (D(x,t)\nabla u) - F(x,t) d\Omega.$$

Taking derivatives on both sides we end up with the *reaction-diffusion equation*, which describes how our tumor changes over time in response to an influx of nutrients:

$$\frac{\partial u}{\partial t} = \nabla \cdot (D(x,t)\nabla u) - F(x,t). \tag{1.12}$$

The reaction-diffusion equation is a well-studied PDE and has widespread application across a variety of scientific disciplines including physics, biology, and the social sciences. The reaction-diffusion equation has been used extensively in cancer modeling, see [9], [45], [51].

1.3.2 CAR-T cell Model

As shown in section 2.2.2, deterministic ODE models describing CAR-T cells require coupling between the tumor cells and the immune cells due to the complex nonlinear interaction between the two cell populations. For the PDE model we require a similar tumor cell lysis term. We introduce a system of two reaction-diffusion equations and modify the $F(x,t)$ term from the reaction-diffusion equation to account for the nonlinear coupling. We let $u(x,t)$ be the density of tumor cells and $v(x,t)$ be the density of CAR-T cells.

$$\frac{\partial u}{\partial t} = \nabla \cdot (D_T(u)\nabla u) + F_1(u,v), \tag{1.13}$$

$$\frac{\partial v}{\partial t} = \nabla \cdot (D_C(u)\nabla v) + F_2(u,v), \tag{1.14}$$

where D_C is the diffusion coefficient for the CAR-T cells and D_T is a piecewise function defined to be:

$$D_T(u) = \begin{cases} 0 & u(x,t) \leq u^* \\ D_T^* & u(x,t) > u^*. \end{cases}$$

This piecewise coefficient models crowding, which is the the tendency for tumor cells in smaller tumors to get bunched up in locations up to a carrying capacity, and once the carrying capacity is met the cells

proliferate outwards toward sparse areas. The nonlinear forcing functions $F_1(u,v)$ and $F_2(u,v)$ are given by

$$
\begin{aligned}
F_1(u,v) &= a(1-bu(x,t))u(x,t) + D(u,v),\\
F_2(u,v) &= j\ln\left(\frac{k}{v(x,t)}\right)\frac{D(u,v)}{k+D(u,v)}v(x,t) - (m+qu(x,t))v(x,t),\\
D(u,v) &= d\frac{\left(\frac{v(x,t)}{u(x,t)}\right)^l}{s+\left(\frac{v(x,t)}{u(x,t)}\right)^l},
\end{aligned}
$$

where a, b, d, l, s, j, k, m, q are the same as in table 1.1. These forcing functions describe the complex non-linear coupling between the tumor and CAR-T cells and are based on the terms from the ODE model 1.11. To derive the dimensionless equations, we use the timescale $T = \frac{1}{a}$ and we let: $\alpha_T = \frac{aR_0^2}{D_C}$, $\alpha_C = \frac{jR_0^2}{D_C}$, $\kappa = \frac{k}{u_*}$, $\beta_T = bu_*$, $\beta_C = \frac{d}{k}$, $\gamma_T = \frac{d}{a}$, $\gamma_C = \frac{qu_*}{j}$, and $\chi = \frac{m}{j}$. Using these parameters, we get the dimensionless system

$$\frac{\partial \tilde{u}}{\partial t} = \nabla\cdot(\tilde{D}_T(u)\nabla u) + \tilde{F}_1(\tilde{u},\tilde{v}), \tag{1.15}$$

$$\frac{\partial \tilde{v}}{\partial t} = \nabla\cdot(\tilde{D}_C(u)\nabla v) + \tilde{F}_2(\tilde{u},\tilde{v}), \tag{1.16}$$

where $\tilde{D}_T(u)$ is now:

$$\tilde{D}_T(u) = \begin{cases} 0 & u(x,t)\le 1 \\ D_T^* & u(x,t) > 1, \end{cases}$$

and the non-linear coupling terms are

$$
\begin{aligned}
\tilde{F}_1(u,v) &= \left[1-\beta_T\tilde{u} - \gamma\frac{\tilde{v}^l}{s\tilde{u}^l+\tilde{v}^l}\right]\tilde{u}(x,t),\\
\tilde{F}_2(u,v) &= \alpha\left[\ln\left(\frac{\kappa}{\tilde{v}}\right)\frac{\tilde{v}^l\tilde{u}}{s\tilde{u}^l+\tilde{v}^l+\zeta_C\tilde{v}^l\tilde{u}}\right]v(x,t).
\end{aligned}
$$

For the remainder of the thesis, we drop the tilde's and u and v will refer to the dimensionless equations 1.15. Due to the highly nonlinear forcing functions in this PDE system, it would not be feasible to search for an analytical solution. Therefore, we look for numerical approximations to the system 1.15.

1.4 Finite Element Approximation of Tumor Models

Tumors are heterogeneous environments - even the same type of tumor can differ greatly between 2 patients [32]. As a consequence, we look for a numerical method that can handle complicated geometries. Since finite differences use square lattices to discretize PDEs, they struggle with more complicated geometries [38]. Spectral methods, while maintaining high accuracy, use basis functions that are globally non-zero on the entire domain. This makes them slower to convergence compared to finite element methods when the domain varies locally. Thus, we will numerically approximate the system 1.15 using the finite element method (FEM) to make it generalizable to the heterogeneous tumors found in clinical patients.

1.4.1 Finite Element Method

The finite element method is one of the most widely used methods of approximating PDEs, and it has found wide application in engineering, physics, and biology. The FEM works by discretizing an n-dimensional domain Ω into an associated mesh by subdividing the domain into n-dimensional polynomials. There are many different ways of subdividing a mesh, and the choice of subdivision will impact the convergence of the solution. A great visual summary of the different families of elements can be found in [2]. We will focus on the Lagrange family of elements. This is the most common family of finite elements and utilizes n-dimensional tetrahedrons as a means of discretizing the mesh. A 2-dimensional example can be found in Fig. 1.5. Let $\Omega \subset \mathbb{R}^n$ be an n-dimensional domain. Let T_h be our mesh, or the set of all n-dimensional tetrahedrons $\mathcal{T}_h$ that discretize the domain. The subscript h is the mesh level, which defines the number of tetrahedrons in our mesh (see Fig. 1.5). The act of subdividing the mesh into tetrahedrons is referred to as a tessellation of Ω. We introduce the definition for a finite element based on Ciarlet [10].

Definition 1. A finite element is a triple $(\mathcal{T}_h, \mathcal{V}_h, \mathcal{L}_h)$ where $\mathcal{T}_h \subset \mathbb{R}^n$ is an n-dimensional polygon, $\mathcal{V}_h \subset H^1(\Omega)$ is a finite dimensional polynomial space on $\mathcal{T}_h$, and $\mathcal{L}_h = \{\ell_0, \ldots, \ell_{n-1}\}$ is the basis of the dual space $\mathcal{V}_h^*$. The basis functions $\{\phi_0, \ldots, \phi_{n-1}\}$ of $\mathcal{V}_h$ satisfy

$$\ell_i(\phi_j) = \begin{cases} 1 & i = j \\ 0 & i \neq j \end{cases}$$

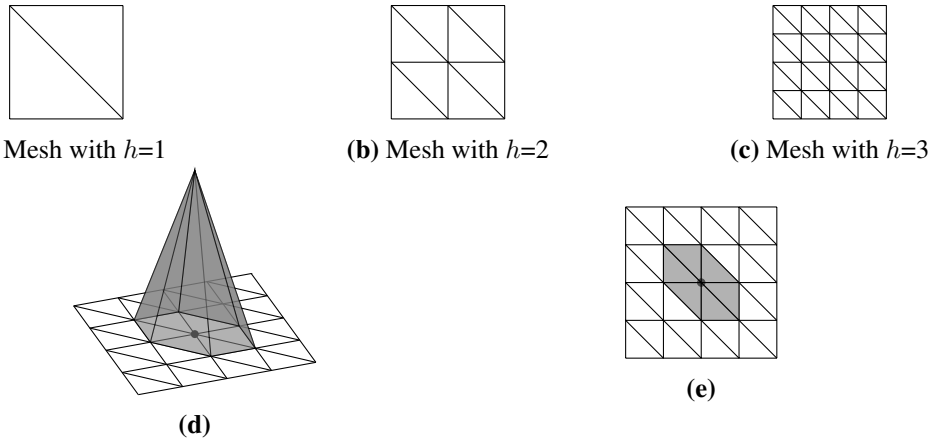

(a) Mesh with h=1 **(b)** Mesh with h=2 **(c)** Mesh with h=3

(d) **(e)**

Figure 1.5: A geometric picture of a 2-dimensional mesh and the associated nodal basis functions. In **a**, **b**, and **c** we see a tessellated square mesh with mesh levels 1, 2, and 3 respectively. In **d** we see a geometric picture of the basis function for Lagrangian order 1 finite elements. The peak of the "tent" function has value 1, and outside the tent the function is 0. **e** shows us a 2D overview of the coordinate patch defined for a single nodal basis function.

Fig. 1.5 shows this definition geometrically for 2 dimensional nodal basis functions on a square mesh of triangles. We utilize the weak form of a PDE in order to discretize. To get the weak form, we simply multiply by a test function $v \in H_0^1(\Omega)$ and integrate over the domain. Once we have specified the finite elements for our domain Ω, we can use the function space to get a discretized version of the weak form of a PDE. Let

$$a(u, v) = L(v),$$
$$u(x, 0) = u_0(x),$$

be a bilinear form representing the weak form of a linear partial differential equation with initial condition $u_0(x)$ and $v \in H_0^1(\Omega)$ arbitrary. Then, we can take $u_h, v_h \in \mathcal{V}_h$ to obtain the discrete approximation to the bilinear form

$$a(u_h, v_h) = L(v),$$
$$u_h(x, 0) = u^0,$$

where u^0 is the L^2 projection of the initial condition $u_0(x)$ onto the finite element space $\mathcal{V}_h$. Since $v_h \in \mathcal{V}_h$

is an arbitrary test function, we let $v_h = \phi_j$. We can then write u_h in terms of nodal basis functions:

$$u_h = \sum_{i=1}^{N} c_i \phi_i,$$

where N is the number of tetrahedrons in our mesh and $c_i \in \mathbb{R}$. Since $a(u_h, v_h)$ is bilinear, we have

$$a(u_h, v_h) = a\left(\sum_{i=1}^{N} c_i \phi_i, \phi_j\right) = \sum_{i=1}^{N} c_i a(\phi_i, \phi_j) = L(\phi_j).$$

This is commonly formatted in terms of an $N \times N$ matrix equation $A\vec{c} = \vec{b}$:

$$\begin{bmatrix} a(\phi_1, \phi_1) & \dots & a(\phi_N, \phi_1) \\ a(\phi_1, \phi_2) & \dots & a(\phi_N, \phi_2) \\ \vdots & \ddots & \vdots \\ a(\phi_1, \phi_N) & \dots & a(\phi_N, \phi_N) \end{bmatrix} \begin{bmatrix} c_1 \\ c_2 \\ \vdots \\ c_N \end{bmatrix} = \begin{bmatrix} L(\phi_1) \\ L(\phi_2) \\ \vdots \\ L(\phi_N) \end{bmatrix}.$$

Solving this equation for $c_1, \dots, c_N$ allows us to reconstruct u_h using the known basis functions. This matrix can be solved using a number of different methods from numerical linear algebra.

If the variational form of the PDE is nonlinear we can't directly achieve a matrix equation to solve for the constants. Instead, we take a linear approximation and use iterative methods to solve for u_h. Let $a(u, v) = L(u)$ be a nonlinear variational form for a PDE with initial condition $u_0(x)$. We put the PDE into the following form

$$F(u, v) = a(u, v) - L(u) = 0.$$

We discretize this equation the same way as the linear FEM case. Let $v_h = \phi_j$ be an arbitrary test function and $u_h = \sum_{i=1}^{N} c_i \phi_i$. Then we get:

$$F(u_h, v_h) = F(\sum_{i=1}^{N} c_i \phi_i, \phi_j) = 0.$$

Since the basis functions are known, this becomes a function of the constants c_i. In order to approximate the solution, we linearize around $u = u_h$ to get a bilinear form $\tilde{F}(u_h, v_h)$ and then use iterative methods to

solve for u_h in the equation $\tilde{F}(u_h, v_h) = 0$.

1.4.2 Variational Form of CAR-T Cell System

We derive the variational form of the system 1.15. Since both equations are in the same form the derivations will be the same, thus we will only show the derivation for the tumor growth equation. Since both equations vary in time, we take a backward Euler approximation to the time derivative

$$\begin{aligned}
&\frac{\partial u}{\partial t} = \nabla \cdot (D_T(u)\nabla u) + F_1(u, v) \\
&\implies \frac{u^{n+1} - u^n}{\Delta t} = \nabla \cdot (D_T(u)\nabla u) + F_1(u, v) \\
&\implies u^{n+1} - u^n = \Delta t \nabla \cdot (D_T(u)\nabla u) + \Delta t F_1(u, v) \\
&\implies u^{n+1} = \Delta t \nabla \cdot (D_T(u)\nabla u) + \Delta t F_1(u, v) + u^n.
\end{aligned}$$

Since u^n is known and u^{n+1} is what we wish to solve for, we let $u^{n+1} = u$. We subtract all the unknown terms to the left hand side:

$$u - \Delta t \nabla \cdot (D_T(u)\nabla u) - \Delta t F_1(u, v) = u^n.$$

Now we derive the weak form by letting $w_1 \in H_0^1(\Omega)$ be an arbitrary test function. We multiply both sides by w_1 and integrate, and we get

$$\int_\Omega u w_1 - \Delta t w_1 \nabla \cdot (D_T(u)\nabla u) - w_1 \Delta t F_1(u, w_1) d\Omega = \int_\Omega u^n w_1 d\Omega.$$

Integrating the second term on the left hand side by parts and noting that the boundary terms are 0 due to Neumann boundary conditions, we can eliminate the divergence and obtain

$$\int_\Omega u w_1 - \Delta t \nabla (D_T(u)u) \cdot \nabla w_1 - w_1 \Delta t F_1(u, w_1) d\Omega = \int_\Omega u^n w_1 d\Omega.$$

This is of the form $a(u, w_1) = L(u)$. We note that when $F_1(u, w_1) = 0$, which corresponds to non-forced tumor growth, we get a bilinear variational form. However, in the CAR-T Cell model, $F_1(u, w_1)$ is highly

nonlinear. Thus, we rewrite in the form:

$$F(u, w_1) = \int_\Omega uw_1 - \Delta t \nabla (D_T(u)u) \cdot \nabla w_1 - w_1 \Delta t F_1(u, w_1) - u^n w_1 d\Omega = 0. \tag{1.17}$$

This is the variational form for the first equation in our CAR-T cell model. Following the same derivation steps and choosing a test function $w_2 \in H_0^1(\Omega)$, we get the analogous variational form for the CAR-T cell equation:

$$F(v, w_2) = \int_\Omega vw_2 - \Delta t \nabla (D_C(v)v) \cdot \nabla w_2 - w_2 \Delta t F_2(v, w_2) - v^n w_2 d\Omega = 0. \tag{1.18}$$

To use the FEM on a system of PDEs, mixed spaces must be used. A mixed finite element space is simply the product space of 2 finite element spaces. The basis functions for the mixed space are defined to be the tensor product of the basis functions for each space. Let $\mathcal{V}_h = \mathcal{V}_h^{(1)} \times \ldots \mathcal{V}_h^{(n)}$ be the product of n finite element spaces, then the basis functions for $\mathcal{V}_h$ are given by

$$\phi_i = \bigotimes_{j=1}^{n} \phi_i^{(j)},$$

where $\phi_i^{(i)}$ is the i-th basis function for the j-th finite element space. Instead of a matrix equation, mixed finite element spaces solve a tensor equation to find the tensor $[c_1^{(1)}, c_2^{(1)}, \ldots, c_N^{(1)}] \otimes [c_1^{(2)}, c_2^{(2)}, \ldots, c_N^{(2)}] \otimes \cdots \otimes [c_1^{(n)}, c_2^{(n)}, \ldots, c_N^{(n)}]$, then apply tensor decomposition methods to obtain the constants corresponding to each finite element space.

1.5 Results

We solve 3 PDEs related to tumor growth using different variations of the finite element method: purely diffusive tumor growth, tumor growth with logistic forcing, and tumor growth with CAR-T cell coupling. We run the finite element method for each case in a unit cube mesh with 30 discrete cells in the x, y, and z directions, corresponding to $6 \times 30^3 = 162000$ tetrahedra and 29791 vertices. We solve each using FeNICS, a python finite element library built on top of Dolfin and UFL. We note that FeNICS currently has an issue in that it will not allow non-integer exponents in the variational formulation, therefore unless otherwise stated

we take $l = 1$. This is a slight biological inaccuracy as l has been measured to be 1.36. More information about these libraries and how they work can be found in [41], [40], [29], [4][26], [5], [20], [54], [28], [18], [19].

1.5.1 Purely Diffusive Tumor Growth

The equation for tumor growth without forcing is given by

$$\frac{\partial u}{\partial t} = \nabla \cdot (D(x,t)\nabla u).$$

This is equivalent to the first equation in the system 1.15 but with $F_1(u,v) = 0$. Using the variational formulation 1.17 with $F_1 = 0$ we get:

$$F(u,v) = \int_\Omega uw - \Delta t D_T(u)\nabla(u)\cdot\nabla(w) - u^n w d\Omega, \tag{1.19}$$

where $w \in H_0^1(\Omega)$ is an arbitrary test function. We note that this PDE is linear and by taking $u_h, w_h \in \mathcal{V}_h$, we get the discrete variational form

$$\begin{aligned} a(u_h, w_h) &= \int_\Omega u_h w_h - \Delta t D_T \nabla(u_h)\cdot\nabla(w_h) d\Omega, \\ L(w_h) &= \int_\Omega u^n w_h d\Omega. \end{aligned}$$

We model this with a constant diffusion source $D_T = 0.00556$ and the initial condition

$$u_0(x) = \begin{cases} 1000 & x,y,z \leq 0.25 \\ 0 & \text{otherwise}, \end{cases} \tag{1.20}$$

The results are shown in Fig. 1.6. We plot a 2-dimensional heatmap of the tumor concentration for the 2-dimensional slice $z = 0$, and show the results at different time steps. We see that after the initial concentration, the tumor starts to spread out symmetrically in all directions.

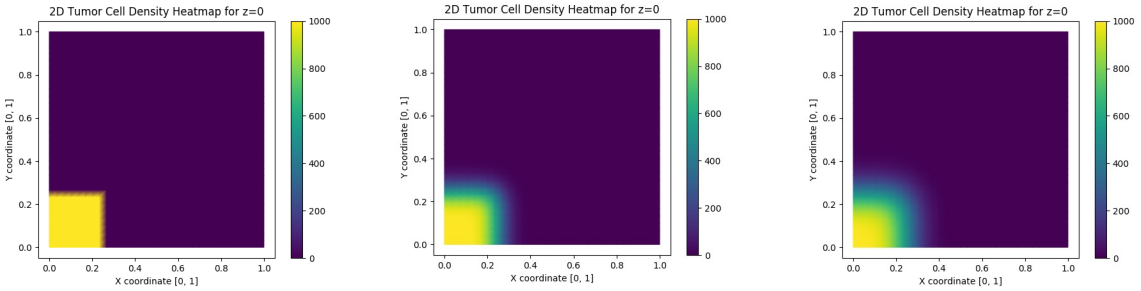

Figure 1.6: Tumor heatmap for the denisty of tumor cells at time steps 0, 12, and 25. We plot the 2-dimensional slice at $z = 0$. We see the initial condition slowly diffuse outward.

1.5.2 Tumor Growth without Forcing

The equation for tumor growth with nonlinear forcing is given by

$$\frac{\partial u}{\partial t} = \nabla \cdot (D(x,t)\nabla u) + F_1(u,v),$$

which is equivalent to system (1.15) but with $v = 0$. This leaves the forcing term as:

$$F_1(u,v) = (1 - \beta_T u)u.$$

This is equivalent to the first equation in the system (1.15) so we can again use the variational formulation (1.17), but with $F_1 = (1 - \beta_T u)u$. We get:

$$F(u,w) = \int_\Omega uw - \Delta t \nabla (D_T(u)u) \cdot \nabla w - w\Delta t(1 - \beta_T u)u - u^n w d\Omega = 0, \tag{1.21}$$

where $w \in H_0^1(\Omega)$ is an arbitrary test function. We note that this PDE is nonlinear, so we have written it in the form $F(u,w) = 0$. As above, we discretize using the Lagrange family of finite elements. Let $u_h, w_h \in \mathcal{V}_h$. The discrete variational form is then

$$F(u,w) = \int_\Omega u_h w_h - \Delta t D_T \nabla (u_h) \cdot \nabla w_h - w_h \Delta t(1 - \beta_T u_h)u_h - u^n w d\Omega = 0. \tag{1.22}$$

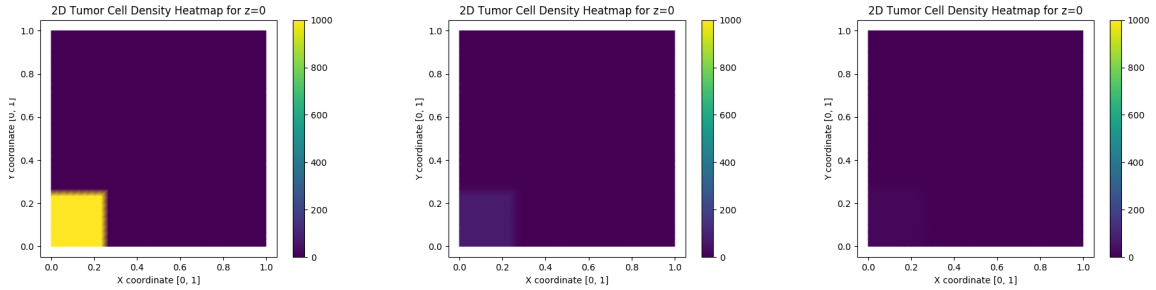

Figure 1.7: Tumor heatmap for tumor cell density at $t = 0, 2, 3$. We see the tumor cells quickly die out to far below the initial condition. In the initial condition, there is a high concetration of tumor cells in the box $x, y, z \leq 0.25$. By the second time step, the nonlinear forcing term has almost completely wiped out the tumor cells, only a small volume of cells remain in the box. By 3 time steps, the tumor looks to be almost wiped out, with no noticable coloring on the heatmap.

We model this with a diffusion source $D_T = 0.00556$, $\beta_t = 4.27256601 \cdot 10^{-9}$, and the initial condition

$$u_0(x) = \begin{cases} 1000 & x, y, z \leq 0.25 \\ 0 & \text{otherwise} , \end{cases} \tag{1.23}$$

The results are shown in Fig. 1.7 and 1.8. We can see the tumor initially decrease due to the forcing term, but over time there is a relapse and the tumor begins to diffuse out again. In 1.7, we plot a heatmap of the tumor at $z = 0$ for 6 different times. We see that after the initial concentration, the forcing term causes the tumor to shrink to near 0 over a few time steps. In 1.8, we plot the total tumor volume over time to show that the tumor starts to relapse, although it has far less concentration than the initial condition. We cannot show the relapse on the heatmap as the concentration is too low to be visible.

1.5.3 Coupled CAR-T Cell Model

For the coupled model, we use the system 1.15

$$\begin{aligned} \frac{\partial u}{\partial t} &= \nabla \cdot (D_T(u)\nabla u) + F_1(u, v), \\ \frac{\partial v}{\partial t} &= \nabla \cdot (D_C(u)\nabla v) + F_2(u, v), \end{aligned}$$

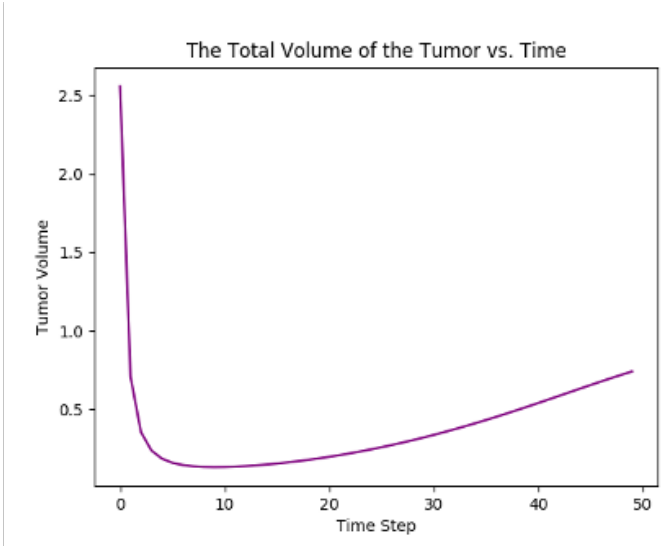

Figure 1.8: Plot of the total volume of the tumor over time. We can see that after a steep drop off in the early time steps, the tumor starts to relapse as the volume increases.

where the forcing functions are given by

$$F_1(u,v) = \left[1 - \beta_T u - \gamma \frac{v^l}{su^l + v^l}\right] u(x,t),$$
$$F_2(u,v) = \alpha \left[\ln\left(\frac{\kappa}{v}\right) \frac{v^l u}{su^l + v^l + \zeta_C v^l u}\right] v(x,t).$$

The variational formulation was derived in equation 1.17 and 1.18

$$F(u,w_1) = \int_\Omega uw_1 - \Delta t \nabla(D_T(u)u) \cdot \nabla w_1 - w_1 \Delta t F_1(u,v) - u^n w_1 d\Omega = 0,$$
$$F(v,w_2) = \int_\Omega vw_2 - \Delta t \nabla(D_C(v)v) \cdot \nabla w_2 - w_2 \Delta t F_2(v,v) - v^n w_2 d\Omega = 0.$$

Using mixed finite element method, we combine these together to form one variational formulation for the mixed space $\mathcal{V}_h \times \mathcal{V}_h$, which is the product space of two identical Lagrange finite element spaces

$$F(u,v;w_1,w_2) = \int_\Omega uw_1 - \Delta t \nabla(D_T(u)u) \cdot \nabla w_1 - w_1 \Delta t F_1(u,v)$$
$$- vw_2 - \Delta t \nabla(D_C(v)v) \cdot \nabla w_2 - w_2 \Delta t F_2(u,v) - v^n w_2 d\Omega = 0.$$

We discretize by letting $u_h, v_h, w_{1,h}, w_{2,h} \in \mathcal{V}_h$[1] and we get the discrete variational form

$$F(u_h, v_h; w_{1,h}, w_{2,h}) = \int_\Omega u_h w_{1,h} - \Delta t \nabla(D_T(u_h)u_h) \cdot \nabla w_{1,h} - w_{1,h}\Delta t F_1(u_h, v_h) \\ - v w_{2,h} - \Delta t \nabla(D_C(v_h)v_h) \cdot \nabla w_{2,h} - w_{2,h}\Delta t F_2(u_h, v_h) - v_h^n w_{2,h} d\Omega = 0.$$

Due to an error in FEniCS, we are unfortunately unable to take non-integer powers in our variational formulation. However, despite this issue, we can still see that the mixed finite element approach allows us to solve the nonlinear coupled CAR-T cell system over 3D geometries. We start by assuming a Gaussian initial condition across the tumor of $u_0(x) = e^{-x^2-y^2-z^2}$. We let $v_0(x)$ be the initial condition for the CAR-T cell injection given by

$$v_0(x) = \begin{cases} 1000 & x, y, z \leq 0.1 \\ 0 & \text{otherwise} \end{cases}$$

The results are shown in Fig. 1.9. We see that over time, the tumor slowly dies out; however, the area of the tumor where there is a large concentration of CAR-T cells dies off noticeably faster than the surrounding area. We see the CAR-T cells slowly diffuse out and begin to die off.

1.6 Conclusion and Discussion

In this chapter, we introduced a spatio-temporal system of partial differential equations to model the nonlinear interaction between tumor cells and CAR-T cells. We solved this system of equations using the finite element method for 3 different cases: purely diffusive tumor growth ($F_1 = F_2 = 0, v = 0$), tumor growth with logistic forcing ($v = 0$), and finally we solved the coupled model using a mixed finite element approach. In each case, we saw convergence using parameters informed by biological data on the unit cube mesh. More work needs to be done to run this system of PDEs over different types of meshes, but this work provides a good starting point and shows the promise of the FEM approach in numerically solving nonlinear PDEs on complex tumors.

For future work, we would like to run the coupled PDE model for different mesh types to get a more

[1]Formally, we are taking some $\chi \in \mathcal{V}_h \times \mathcal{V}_h$ such that $\chi = u_h \otimes v_h$ and $w \in \mathcal{V}_h \times \mathcal{V}_h$ such that $w = w_1 \otimes w_2$, but the end result is the same: $u_h, v_h, w_1, w_2 \in \mathcal{V}_h$

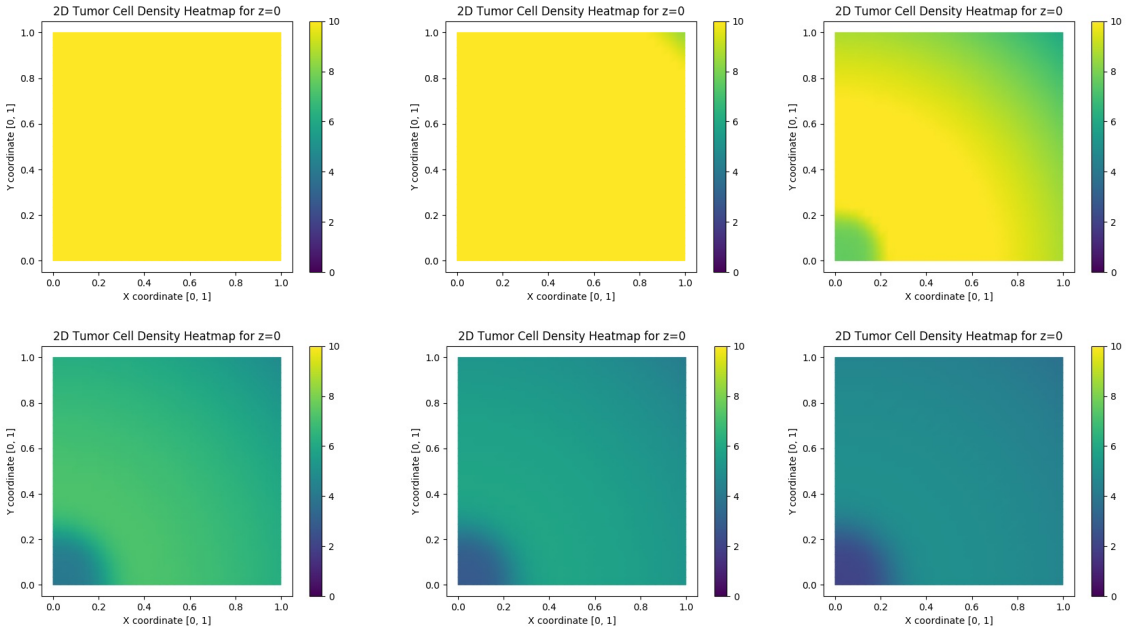

Figure 1.9: Tumor heatmap for tumor cell density for the coupled CAR-T cell model. We plot 6 different time steps: $0, 6, 12, 18, 24, 30$. We see that the tumor cell density decreases overall; however it decreases much faster in the area where CAR-T cells are injected. Even after the CAR-T cells have been wiped out (see Fig 1.10), the area still dies off quicker, going from green to purple faster than the surrounding section.

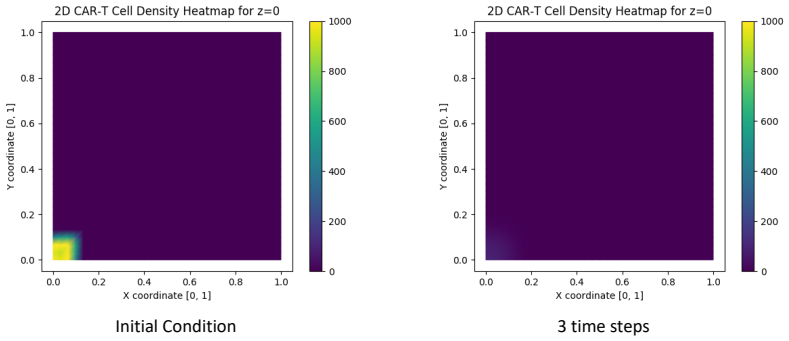

Figure 1.10: CAR-T cell heatmap for CAR-T cell density. We see that the CAR-T cells very quickly go to 0, but the initial injection has a big effect on the local area in the tumor (see Fig. 1.9). Since the CAR-T cells die off very quickly, we only plot 2 time steps: one where there is a visible number of CAR-T cells and the first time step in which there is no easily visible color change to denote the concentration.

biologically accurate picture of how the model behaves on different kinds of tumors. We would also like to derive more theoretical results from finite element methods, such as error bounds and convergence rates. Finally, we would be interested in utilizing a neural network approach to learn the underlying Green's function for our system. This would allow us to directly solve the PDE for any arbitrary tumor type without needing to worry about convergence which would be incredibly useful for analysis on real patient data where tumor geometries can often be very complex.

Chapter 2

Dynamic Modeling of Viral Tweets

2.1 Introduction

Over the last 10 years, misinformation has become a major topic of conversation in the social sciences. It has played a major role in the 2016 and 2020 election cycles as well as the COVID-19 pandemic, with some scientists even saying misinformation is pervasive enough to be considered a crisis discipline on the scale of climate change [6]. As such, it has become imperative that we understand how and why information spreads online. Many mathematical models have been introduced to shed some light on this phenomenon. Such models include compartmental model approaches [17], [31], [16], Ising models from statistical physics [25], and agent based approaches to opinion formation on networks [13], [8]. While these approaches can give a lot of insight into how and why information spreads, it can be difficult to compare these abstract formulations directly with data.

When a piece of content undergoes explosive, exponential growth it is said to have gone viral. In order to understand how misinformation spreads online, it's important to have an accurate model for this category of content. Many medical professionals say that viral vaccine misinformation is one of the biggest public health threats of the 21^{st} century [48], [39], and the viral spread of misinformation by bots played a significant role in the 2016 election [43], [24]. In this chapter, we focus specifically on modeling viral content from Twitter, one of the world's largest social media sites by daily active users and one of the largest propagators of misinformation on the internet. On Twitter, content is shared through retweeting, a mechanism that allows a

piece of content to be shared to all of the retweeter's followers. The cumulative time series for retweets on a single tweet is called a retweet cascade.

The literature for modeling and forecasting viral content on Twitter is vast. In [50], the authors considered an approach based on community structure in networks to predict whether a Twitter meme had become viral. Zhao et al. [53] introduced a statistical model based on self-exciting point processes to predict the final popularity of a tweet. Many statistical models have been utilized that forecast popularity based on tweet content, such as hastags. These include approaches based on Bayesian analysis [52], [30] and linear regression [35], [47]. A discrete approach has been considered by Bak-Coleman et al. in [7]; however, their model was derived through statistical methods and seeks to model cumulative engagement across entire event cycles, such as political elections. Finally, the RC-Tweet model used a continuous model analogous to equations used in circuit analysis to model retweet cascades [27].

In this chapter, we introduce a discrete dynamical system to accurately model retweet cascades. This discrete dynamical system relies entirely on growth parameters that can be estimated using least-squares methods without needing to look at lifetime tweet data. We show that using statistical approaches based in extreme value theory, the model accuracy can be significantly improved by accounting for retweeters that have an exceptionally large follower count. This model maintains high accuracy across the 10 most viral retweets from our dataset and has a lot of potential to inform interventions on Twitter to reduce the spread of viral misinformation.

2.2 The Retweet Model

We introduce a deterministic model that is based on classical birth-death population growth models in population biology. Since the number of individuals undoing their retweets is negligible, we do not have an analogous death term for our equation. In order to obtain the logistic growth we see in the tweet data (see Fig. 2.1), we introduce a simple discrete dynamical equation V_t called the virality that decays in time. Virality is a hidden variable that encodes information about how viral a tweet is. This verbiage was introduced in [7]. We then introduce the discrete equation S_t, which is the cumulative number of retweets at a time t. We consider retweets to be an exponential function of the virality V_t. This accounts for the logistic growth

that we see in the data. Our final model can be written

$$S_{t+1} = \alpha \left(e^{\beta V_{t+1}} - \frac{1}{V_{t+1} - 1} \right), \tag{2.1}$$

$$V_{t+1} = \delta V_t + \ln \left(e^{-\frac{1}{F_0 - 1}} + (1 - e^{-1}) \right), \tag{2.2}$$

where α, β are unknown parameters describing the growth of the retweet cascade, $0 < \delta < 1$ is the virality parameter that determines how quickly virality decays, and F_0 is the initial number of followers for the user who tweeted. We let $V_0 = 0$ and for simplicity we let $\gamma = \ln \left(e^{-\frac{1}{F_0 - 1}} + (1 - e^{-1}) \right)$. Here, γ has been written so that when $F_0 = 0$ the virality term remains at 0 as it would be effectively impossible to propagate a tweet with 0 followers. By setting $\delta < 1$, we assure that V_t decays in time, and thus the growth of S_t slows in time, giving us the logistic growth we see in the data. This set of equations has a fixed point that we obtain by letting $V_{t+1} = V_t = V^*$ and solving for V^*. Solving this equation, we get the fixed point

$$V^* = \frac{\gamma}{1 - \delta}, \tag{2.3}$$

and thus, the fixed point for S_{t+1} is

$$S^* = \alpha \left(e^{\frac{\beta\gamma}{1-\delta}} - \frac{1 - \delta}{\gamma - \delta - 1} \right). \tag{2.4}$$

As a consequence, if we can estimate the parameters α, β, and δ we obtain an estimate for the final number of retweets. This implies that our system is inferring the carrying capacity of the logistic curve based solely on growth parameters, which can be estimated without needing to look at the entire retweet cascade.

2.2.1 Parameter Estimation

Given a sequence of data points $\hat{y}_1, \ldots, \hat{y}_n$ in our data for the retweet cascade, we wish to determine the parameters α, β, and δ. Since this is an underdetermined system of 2 equations with 3 unknowns, we need to utilize special methods to determine our parameters. For these equations, we use nonlinear least-squares

fitting. We look to minimize the equation:

$$F(\hat{\alpha}, \hat{\beta}, \hat{\delta}) = \min_{\hat{\alpha},\hat{\beta},\hat{\delta}} \sum_{t=1}^{N} ||S_t(\hat{\alpha}, \hat{\beta}, \hat{\delta}) - \hat{y}_t||^2, \tag{2.5}$$

where $S_i(\hat{\alpha}, \hat{\beta}, \hat{\delta})$ is the i^{th} predicted retweet, $\hat{y}_i$ is the i^{th} retweet coming from our data, and $\hat{\alpha}, \hat{\beta}, \hat{\delta}$ are the estimated parameters. Since the data points correspond to a time series, we use the subscript t to indicate that the data points and the predicted function are indexed by time. The function notation is being used to indicate that we are varying the parameters in S_t in order to minimize the error.

2.2.2 Results

We now present the results for our model on retweet time series data. For our analysis, we used the top 10 most retweeted tweets in the Cornell Climate Change dataset [1]. This dataset contains retweet information as a time series as well as information about each user who retweeted, such as follower and friend counts. We use the scipy `least_squares()` function to do our parameter estimation. We compute the root mean squared error (RMSE), mean absolute percentage error (MAPE), and R^2 correlation coefficient (R^2) between our fitted model and the data. Table 2.1 shows these error values for each of the 10 retweets, and Fig. 2.1 shows a few of the model fits graphically. We also show the residual error between the last data point and the last predicted point as a means of quantifying whether or not we capture the long term behavior. This is denoted FRE for "final residual error" in the table.

Error Results for Retweet Model on Top Ten Most Retweeted Tweets				
Tweet ID	RMSE	MAPE	R^2	FRE
1066155330986541058	12.9384	3.41%	0.997	141.8472
1067149009867878400	10.1407	7.04%	0.9908	120.8795
1065274149461987328	9.4115	11.36%	0.9941	155.1605
1069278755041001472	8.5322	7.95%	0.9972	48.1857
1069686443109466113	11.4633	31.69%	0.9788	59.2932

1068113206525202433	8.0642	15%	0.9957	11.1861
1069700156067594240	7.4095	4.31%	0.9896	80.1939
1064191037571297280	7.6306	10.01%	0.9927	59.9518
1068595221188042753	6.032	2.82%	0.9954	22.1765
1066352623358361600	4.7473	3.08%	0.9986	19.2811
Averages:	8.6370	9.667%	.9930	71.8156

Table 2.1: The results of fitting the retweet model (2.2) to the top ten most retweeted tweets in our dataset.

We see R^2 correlation values that show a high level of correlation between our predicted model and the data. We also see relatively low values for RMSE and MAPE, implying that our model is capturing the global qualities of the data effectively. However, we do see that while some of our models capture long term accuracy well, some of them are more than a 100 retweets off the final estimated value. This is not terrible considering all of these tweets obtained a significant number of retweets, but we would like to improve our error estimates. We will try to remedy some of these accuracy issues in the following section by considering the idea of superusers.

2.3 Superusers

As seen in the figures and results from the previous section, the retweet cascade is somewhat noisy. There are jumps in the time series and places where the curve seems to taper off but then bumps up again. If we superimpose the retweet time series on top of a time series displaying the maximum number of followers per user at each 5 minute time step, we see that there might be a relationship between the max number of followers and the deviations from a simple logistic growth curve.

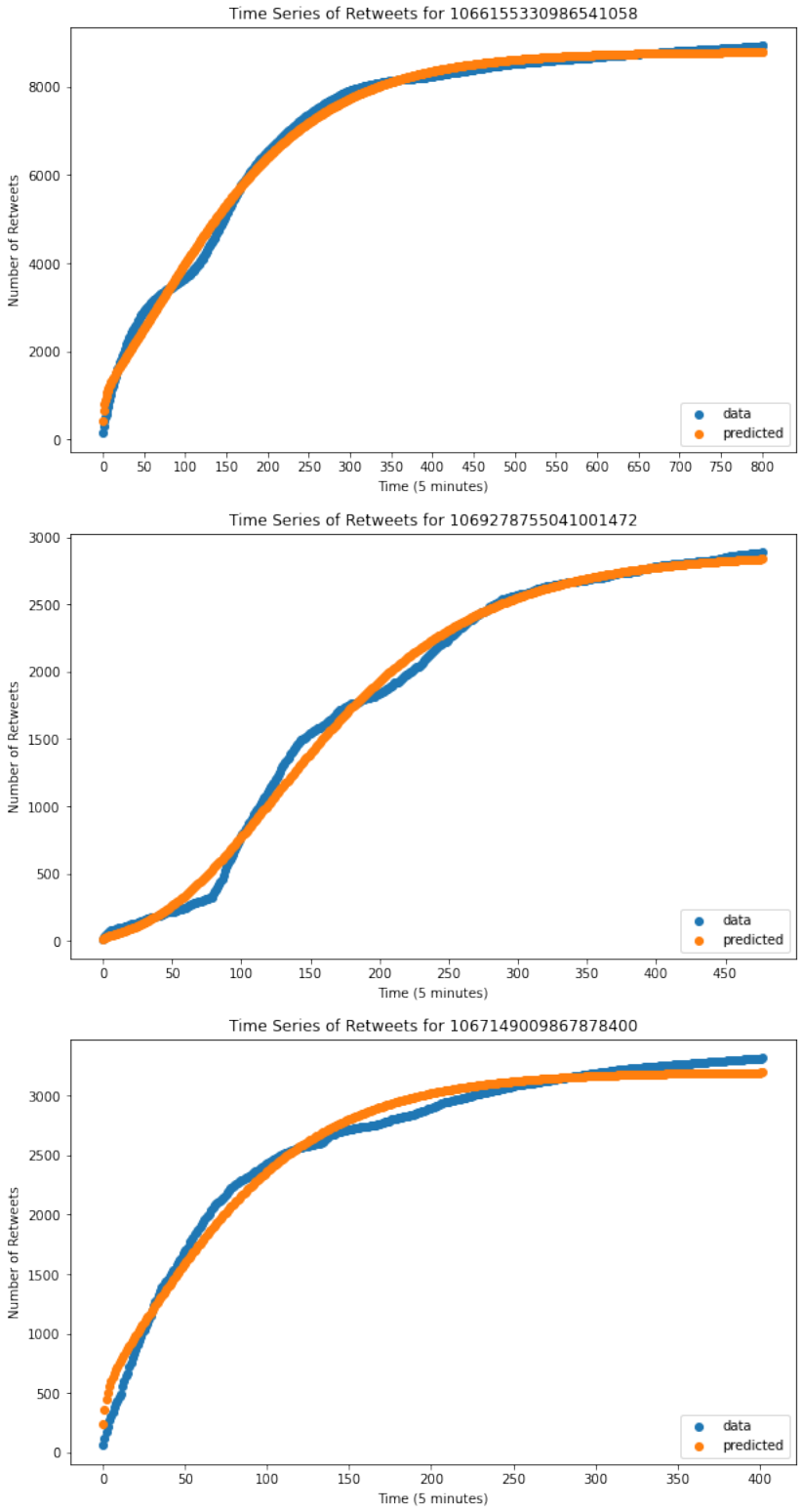

Figure 2.1: Actual retweet time series vs. predicted retweet time series for a few viral tweets in the dataset. The x-axis is measured in 5-minute intervals, so 100 corresponds to 500 minutes.

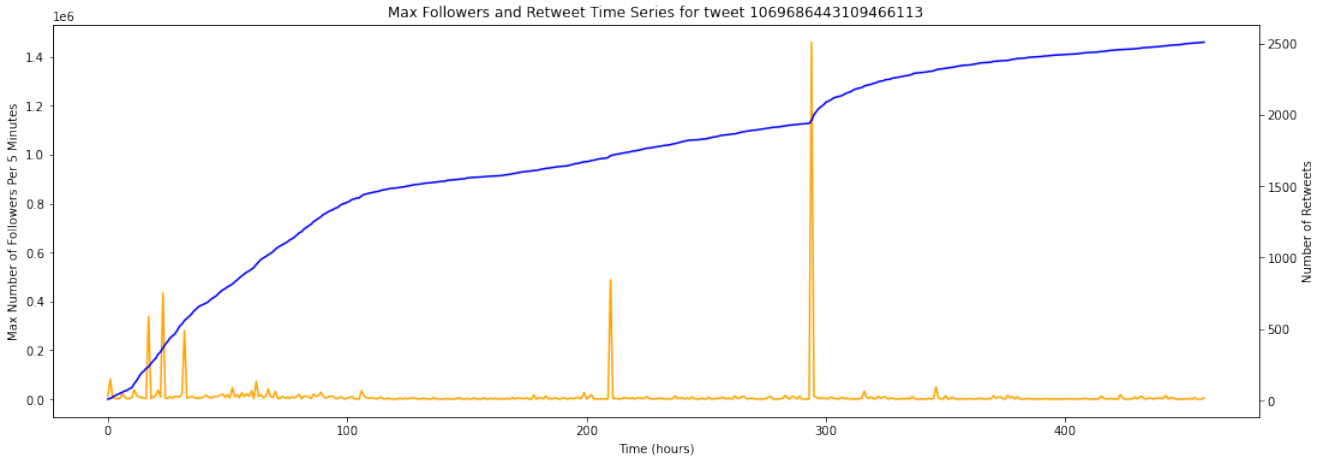

Figure 2.2: Max number of followers at each time step measured in millions vs. the retweet time series. We see that large deviations in the max followers time series corresponds to deviation in the logistic growth of the retweet cascade. Tweet ID = 1069686443109466113

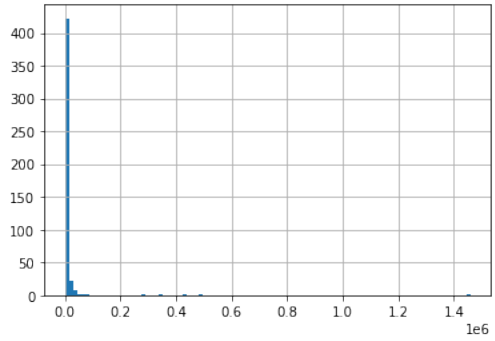

Figure 2.3: Histogram of the max number of followers for each 5 minute interval for tweet 1069686443109466113.

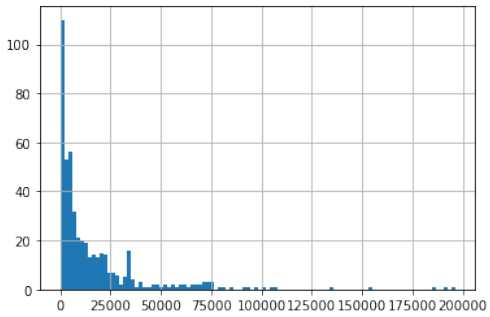

Figure 2.4: Histogram of the max number of followers for each 5 minute interval for tweet 1069278755041001472.

Looking at Fig. 2.2, the y-axis on the left hand side corresponds to the maximum number of followers for a retweeter per 5 minute interval. The right hand side is the number of retweets per 5 minute interval. In 2.2, we can see clearly that the large fluctuations in the max followers correspond to jumps in the retweet time series. In Figs 2.3 and 2.4, we show the histogram plot of max followers per 5 minute interval for 2 tweets showing that follower counts in the time series are very over-dispersed, with the majority of retweeters in the lowest bins and relatively few in the higher bins. Based on this, we hypothesis that the bumps in the retweet cascade are caused by retweeters with large follower counts far above the median that are causing a huge influx in new users and resulting in far more retweets at the next time step. This effectively means that each

retweeter with extremely high follower counts can be modeled as their own tweet, as they have a significant effect on the growth parameters. We refer to these individuals with high follower counts as *superusers*. Our goal is to analyze the large fluctuations in the follower time series to get a probability distribution to describe superusers.

2.3.1 Extreme Value Theory

In order for us to analyze the effect that superusers have on the spread of viral tweets, we turn to a branch of statistics known as extreme value theory (EVT). The goal of EVT is to find limiting distributions for the values in a dataset that deviate far away from the mean [23]. EVT has found use in a wide range of applications including finance, insurance, weather forecasting, and even predicting the height of buildings. For our purposes, we will use EVT to analyze the time series of followers per retweeter. That is, a time series where each data point corresponds to the number of followers of a single retweeter at the time they retweeted the tweet.

2.3.2 Extreme Value Distributions

We restate the main theorem of interest from EVT. The statement of the theorem comes from EVT textbook [23].

Theorem 1. *The class of extreme value distributions is*

$$G_\xi(s) = \exp\left(-(1+\xi s)^{-1/\xi}\right), 1+\xi s > 0, \tag{2.6}$$

with γ real and where for $\gamma = 0$ the right-hand side is interpreted as $e^{-e^{-s}}$ and $s = \frac{x-\mu}{\sigma}$ where μ is the location parameter and $\sigma > 0$ is the scale parameter.

We omit the proof here, but refer to the text [23] for the full proof. This theorem tell us that any sequence of extreme values will tend to equation (2.6) as the number of extreme values in our dataset goes to ∞. This is analogous to the central limit theorem in classical statistics. The goal of our extreme value analysis is to determine ξ and s (μ can be any real number). Once these parameters are determined, the CDF and the PDF for the extreme value distribution follow easily from the theorem.

2.3.3 Peak-Over-Threshold Model

To extract the extreme values from our follower time series, we use the *peak-over-threshold* (POT) model. The POT model works by selecting all values of a time series that exceed a certain *threshold*. Once those values are found, the POT model clusters all the data points by time intervals and selects the maximum from each time interval. We use these data points as our samples to fit to an extreme value distribution. For our purposes, we will be using pyextreme, a python library that aids in performing extreme value analysis [3].

In order to use the peak-over-threshold model for a follower time series, we first need to choose an appropriate threshold value. An approach to choosing a threshold is to plot the mean residual life. This means that we vary the threshold along the x-axis and plot the average excess value over that threshold on the y-axis. In Fig. 2.5, we plot this for three tweet id's 1066155330986541058, 1069278755041001472, 1069686443109466113. In each of these plots, we see that the mean excess increases with the threshold value, since as the threshold gets higher, the number of data points that exceed that threshold decreases, leaving only the very large values. This also explains the increasing variance and the stepwise motion. To choose a good threshold value, we look for areas that are approximately linear above a certain value. This value becomes the threshold. In each of these graphs, we see that at 20,000 the mean excess is roughly linear. To save space, the other 7 graphs have been omitted, but each graph is roughly linear in the 20,000 range. Thus, 20,000 is our first guess for the threshold.

Another method of determining the appropriate threshold is parameter stability. Parameter stability varies the threshold value and fits an extreme value distribution for each threshold. We look for places along the graph where the threshold value is relativity stable, i.e., varies by a small amount, to inform our choice of threshold. If a region on the graph is not stable, that means a small change in the threshold yields a large change in the extreme value distribution. Since we want our threshold to give us a stable distribution, we need to ensure we choose a threshold in a region of stability. In Fig. 2.6 we have plotted the parameter stability for the tweet id 1066155330986541058. We see in the figure that the area with the least variance (i.e., most stable) begins around 20,000 for both parameters. Plotting the parameter stability for each retweet in our time series, we see that there is a stable region around 20,000 in each graph. Therefore, we conclude that 20,000 is a good estimate for the threshold.

Using the threshold of 20,000, we can now use pyextreme to determine the shape and scale parameters

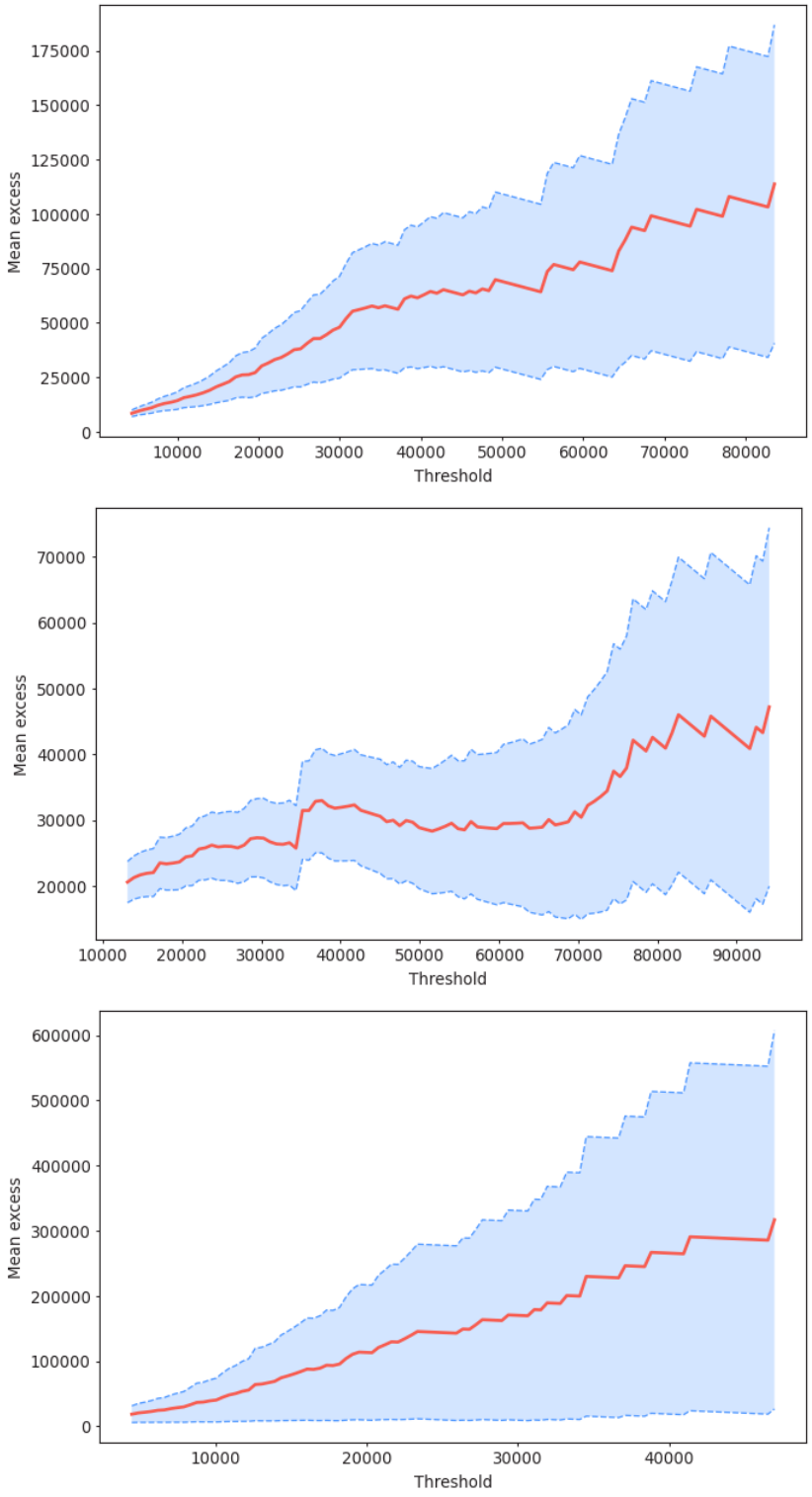

Figure 2.5: Mean residual life plots for 1066155330986541058 (top), 1069278755041001472 (middle), 1069686443109466113 (bottom).

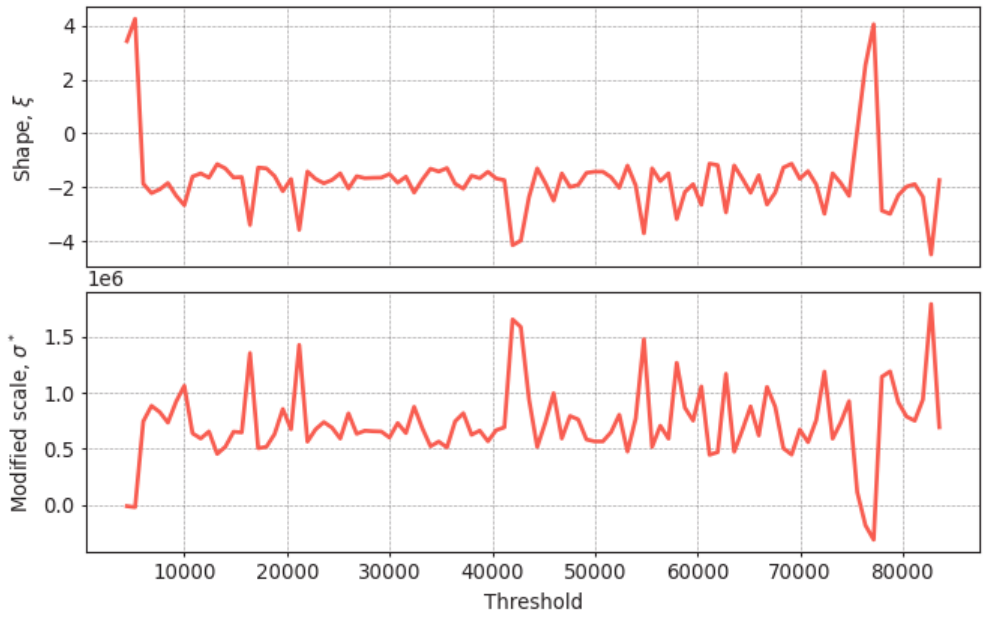

Figure 2.6: Parameter stability plots for Tweet 1066155330986541058.

by using a Markov Chain Monte Carlo method. In Fig. 2.7, we have plotted probability density functions on the top row for the 3 tweet IDs used in this section. We have also displayed Q-Q plots showing the correlation between the residual error of our follower data and the estimated distribution based on the shape and scale parameters. The Q-Q plots show that the residual errors have a high correlation to a Gaussian distribution, meaning that up to white noise, our data fits an extreme value distribution. We do see larger values fluctuate away from the normal line, but this can be explained by not having enough data in between the very large extreme values and the smaller extreme values. From the pdf, we can determine the probability that a specified user will have enough followers to be considered a superuser.

2.3.4 Accounting for Superusers

Lastly, we want to use our analysis on superusers to get a more accurate dynamic model. For each of our top 10 most retweeted tweets, we ran an extreme value analysis using a threshold of 20,000 to get an extreme value distribution for the corresponding follower time series. We determined which users were superusers by how far above the extreme value median they were, in this case we looked for users that were greater than 4 standard deviations above the median of the extreme value distribution. We then treated each retweet from

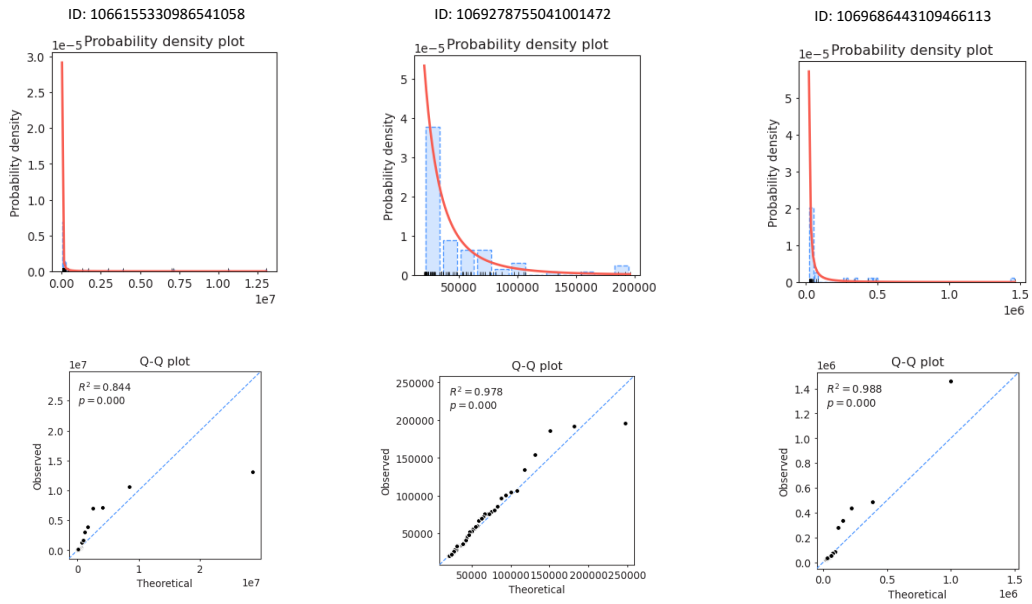

Figure 2.7: Probability density and Q-Q plots showing the extreme value distribution and Q-Q plot of the fit for 3 different tweets in our dataset. We can see extremely varied histograms; some are extremely over dispersed with upper bins in the millions, while the middle plot is less varied. However, the 20,000 threshold manages to produce an extreme value distribution with high correlation for each follower histogram.

a superuser as if it were a new tweet by rerunning the least squares parameter estimation at the time where a superuser retweets the tweet up until the next superuser, or until the end of the tweet if none is found. We then stitch the tweet before and after each superuser to form one prediction. The error results from the analysis are shown below in table 2.2, and some graphical results are shown in Fig. 2.8.

Results for Superuser Model on Top Ten Most Retweeted Tweets				
Tweet ID	RMSE	MAPE	R^2	FRE
1066155330986541058	8.0415	1.09%	0.9996	8.5866
1067149009867878400	4.1701	1.15%	0.9998	14.1446
1065274149461987328	3.5832	.082%	0.9999	12.4618
1069278755041001472	5.1802	3.36%	0.9996	31.3567
1069686443109466113	4.0602	1.67%	0.9997	24.7479
1068113206525202433	3.8691	1.43%	0.9998	14.0503
1069700156067594240	7.497	4.26%	0.9889	85.6555
1064191037571297280	3.8869	1.56%	0.9995	0.9076
1068595221188042753	6.4604	3.36%	0.9939	29.3616
1066352623358361600	3.1524	1.46%	0.9998	1.8565
Averages:	4.9901	1.9422%	.9981	22.3129

Table 2.2: Results for running a model fit using the retweet model (2.2) but treating each superuser independently.

We see a large decline across each error metric when taking superusers into account. Notably, we capture the long term behavior far better, with only being roughly 22 retweets off on average. We see that across all 10 tweets we have an extremely high correlation between the prediction and the data. Not only does this analysis show that retweet cascades can be modeled to a high degree of accuracy deterministically by considering superusers, it also exposes how much of a role superusers play when it comes to spreading viral content online.

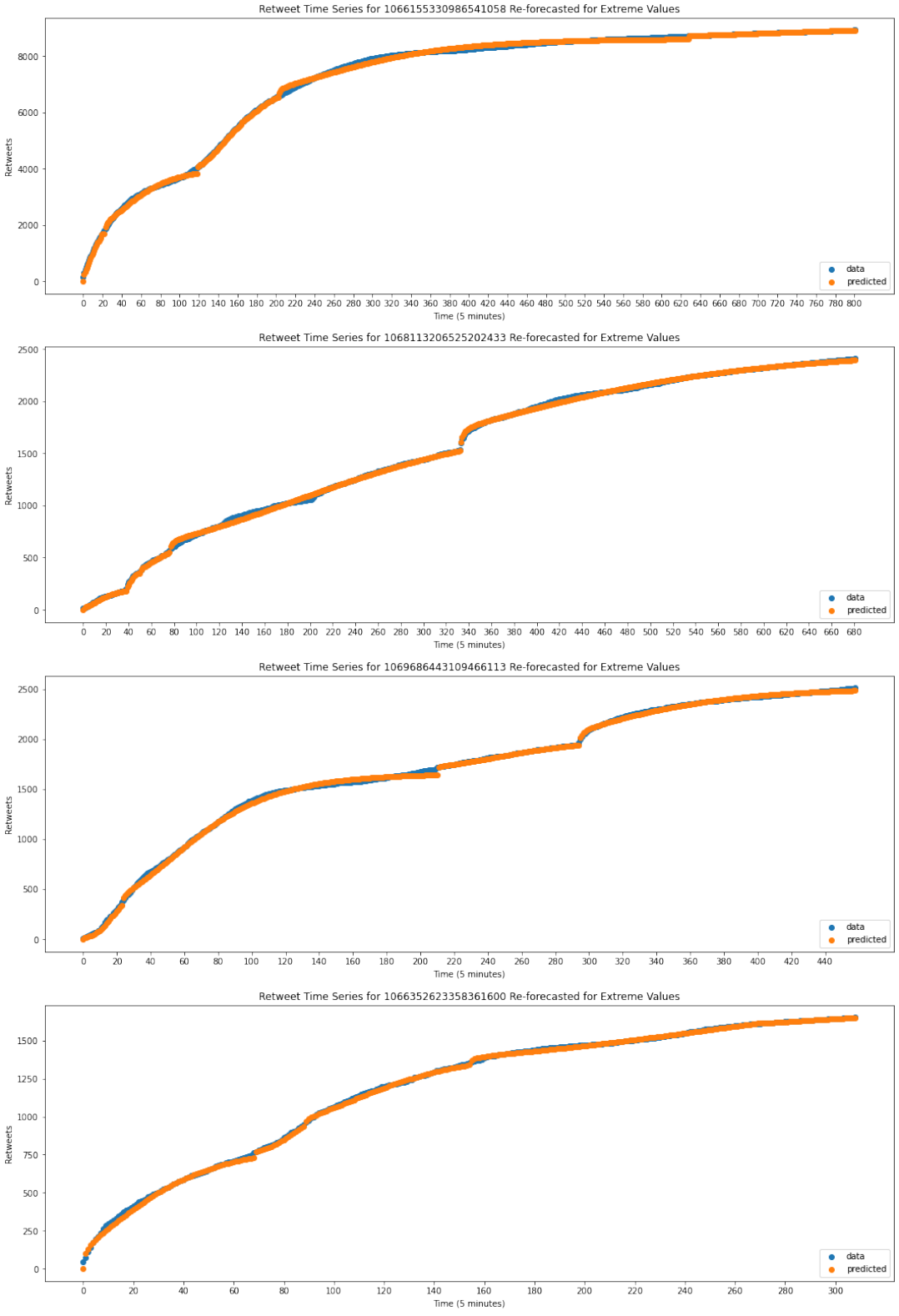

Figure 2.8: 4 tweets from the dataset that have been modeled based on the superuser approach using Extreme Value Theory.

2.4 Conclusions and Discussion

In this chapter, we introduced a discrete dynamical system to model retweet cascades. We showed that a discrete dynamical systems approach can give high correlation and capture long term behavior on the top 10 most viral retweets in our dataset. We then made use of extreme value theory to determine which retweeters in our time series were influential enough to have a significant impact on the overall number of retweets, and used these values to improve the accuracy of our model. In doing this, we achieved significantly improved metrics across our 10 tweets.

The effect of superusers on the retweet cascade is substantial. As a case study, we looked at tweet 1069278755041001472. The user who tweeted this tweet was flagged by Twitter as violating their content policy by spreading misinformation and their account was subsequently given a permanent ban. For reference, this tweet was plotted in Fig. 2.1. Our model shows that the initial tweet, before the influence of the first superuser, was only projected to obtain 78 retweets. This tweet had 4 superusers that aided in information spread, and by the end of the tweet lifecycle it had secure 2800 retweets in total. Intriguingly, none of the superusers who retweeted the tweet have been banned for violating Twitter's content policy, despite having a significant effect on the spread of the viral misinformation. Our model shows that, for the tweets in our dataset, a significant decrease in the spread of information could be attained by reducing the influence of superusers. Thus, a good direction for future intervention efforts in reducing the spread of viral misinformation might lie in reducing the role of superusers in retweet cascades.

For future work, we would be interested in using our extreme value analysis to create a stochastic branching process model like the types considered in cancer modeling. Such a model could be useful for forecasting the spread of information in real-time based on available data, similar to weather forecasting. We would also like to consider machine learning methods to determine the extreme values in the follower time-series in real-time. Both of these projects could provide useful insights into how we should detect and reduce viral misinformation.

Bibliography

[1] Cornell Virtual Workshop: Twitter Data.

[2] Periodic Table of the Finite Elements.

[3] pyextremes.

[4] G. N. W. A. Logg and J. Hake. DOLFIN: a C++/Python finite element library. In K. M. A. Logg and G. N. Wells, editors, *Automated Solution of Differential Equations by the Finite Element Method*, volume 84 of *Lecture Notes in Computational Science and Engineering*, chapter 10. Springer, 2012.

[5] M. E. R. A. Logg, K. B. Ølgaard and G. N. Wells. FFC: the FEniCS form compiler. In K. M. A. Logg and G. N. Wells, editors, *Automated Solution of Differential Equations by the Finite Element Method*, volume 84 of *Lecture Notes in Computational Science and Engineering*, chapter 11. Springer, 2012.

[6] J. B. Bak-Coleman, M. Alfano, W. Barfuss, C. T. Bergstrom, M. A. Centeno, I. D. Couzin, J. F. Donges, M. Galesic, A. S. Gersick, J. Jacquet, A. B. Kao, R. E. Moran, P. Romanczuk, D. I. Rubenstein, K. J. Tombak, J. J. Van Bavel, and E. U. Weber. Stewardship of global collective behavior. *Proceedings of the National Academy of Sciences*, 118(27):e2025764118, July 2021.

[7] J. B. Bak-Coleman, I. Kennedy, M. Wack, A. Beers, J. S. Schafer, E. Spiro, K. Starbird, and J. West. Combining interventions to reduce the spread of viral misinformation, May 2021.

[8] F. Baumann, P. Lorenz-Spreen, I. M. Sokolov, and M. Starnini. Modeling echo chambers and polarization dynamics in social networks. *Physical Review Letters*, 124(4):048301, Jan. 2020. arXiv:1906.12325 [physics].

[9] Y. Chen and J. S. Lowengrub. Tumor growth in complex, evolving microenvironmental geometries: A diffuse domain approach. *Journal of theoretical biology*, 361:14–30, Nov. 2014.

[10] P. G. Ciarlet. *The Finite Element Method for Elliptic Problems*. Classics in Applied Mathematics. Society for Industrial and Applied Mathematics, Jan. 2002.

[11] L. G. de Pillis, A. E. Radunskaya, and C. L. Wiseman. A Validated Mathematical Model of Cell-Mediated Immune Response to Tumor Growth. *Cancer Research*, 65(17):7950–7958, 09 2005.

[12] Y. Dong, R. Miyazaki, and Y. Takeuchi. Mathematical modeling on helper t cells in a tumor immune system. *Discrete and Continuous Dynamical Systems - B*, 19(1):55–72, 2014.

[13] D. Geschke, J. Lorenz, and P. Holtz. The triple-filter bubble: Using agent-based modelling to test a meta-theoretical framework for the emergence of filter bubbles and echo chambers. *The British Journal of Social Psychology*, 58(1):129–149, Jan. 2019.

[14] D. Hardiansyah and C. M. Ng. Quantitative Systems Pharmacology Model of Chimeric Antigen Receptor T-Cell Therapy. *Clinical and Translational Science*, 12(4):343–349, July 2019.

[15] B. Hopkins, M. Tucker, Y. Pan, N. Fang, and Z. J. Huang. A Model-Based Investigation of Cytokine Storm for T-Cell Therapy. *IFAC-PapersOnLine*, 51(19):76–79, Jan. 2018.

[16] F. Jin, E. Dougherty, P. Saraf, Y. Cao, and N. Ramakrishnan. Epidemiological modeling of news and rumors on Twitter. In *Proceedings of the 7th Workshop on Social Network Mining and Analysis - SNAKDD '13*, pages 1–9, Chicago, Illinois, 2013. ACM Press.

[17] J. Kauk, H. Kreysa, and S. R. Schweinberger. Understanding and countering the spread of conspiracy theories in social networks: Evidence from epidemiological models of Twitter data. *PLoS ONE*, 16(8):e0256179, Aug. 2021.

[18] R. C. Kirby. Algorithm 839: FIAT, a new paradigm for computing finite element basis functions. *ACM Transactions on Mathematical Software*, 30:502–516, 2004.

[19] R. C. Kirby. FIAT: numerical construction of finite element basis functions. In K. M. A. Logg and G. N.

Wells, editors, *Automated Solution of Differential Equations by the Finite Element Method*, volume 84 of *Lecture Notes in Computational Science and Engineering*, chapter 13. Springer, 2012.

[20] R. C. Kirby and A. Logg. A compiler for variational forms. *ACM Transactions on Mathematical Software*, 32, 2006.

[21] D. Kirschner and J. C. Panetta. Modeling immunotherapy of the tumor – immune interaction. *Journal of Mathematical Biology*, 37(3):235–252, Sept. 1998.

[22] V. A. Kuznetsov, I. A. Makalkin, M. A. Taylor, and A. S. Perelson. Nonlinear dynamics of immunogenic tumors: Parameter estimation and global bifurcation analysis. *Bulletin of Mathematical Biology*, 56(2):295–321, Mar. 1994.

[23] H. Laurens and F. Ana. *Extreme Value Theory*.

[24] T. Lee. The global rise of "fake news" and the threat to democratic elections in the USA. *Public Administration and Policy*, 22(1):15–24, Jan. 2019. Publisher: Emerald Publishing Limited.

[25] C. Li, F. Liu, and P. Li. Ising Model of User Behavior Decision in Network Rumor Propagation. *Discrete Dynamics in Nature and Society*, 2018:e5207475, Aug. 2018. Publisher: Hindawi.

[26] A. Logg and G. N. Wells. DOLFIN: automated finite element computing. *ACM Transactions on Mathematical Software*, 37, 2010.

[27] I. N. Lymperopoulos. RC-Tweet: Modeling and predicting the popularity of tweets through the dynamics of a capacitor. *Expert Systems with Applications*, 163:113785, Jan. 2021.

[28] J. H. A. J. B. K. A. L. C. R. J. R. M. E. R. M. S. Alnaes, J. Blechta and G. N. Wells. The FEniCS project version 1.5. *Archive of Numerical Software*, 3, 2015.

[29] K. B. M. E. R. M. S. Alnaes, A. Logg and G. N. Wells. Unified form language: A domain-specific language for weak formulations of partial differential equations. *ACM Transactions on Mathematical Software*, 40, 2014.

[30] Z. Ma, A. Sun, and G. Cong. On predicting the popularity of newly emerging hashtags in Twitter. *Journal of the American Society for Information Science and Technology*, 64(7):1399–1410, 2013. _eprint: https://onlinelibrary.wiley.com/doi/pdf/10.1002/asi.22844.

[31] M. Maleki, E. Mead, M. Arani, and N. Agarwal. Using an Epidemiological Model to Study the Spread of Misinformation during the Black Lives Matter Movement. Technical Report arXiv:2103.12191, arXiv, Mar. 2021. arXiv:2103.12191 [cs] type: article.

[32] A. Marusyk and K. Polyak. Tumor heterogeneity: Causes and consequences. *Biochimica et Biophysica Acta (BBA) - Reviews on Cancer*, 1805(1):105–117, 2010.

[33] A. N. Miliotou and L. C. Papadopoulou. CAR T-cell Therapy: A New Era in Cancer Immunotherapy. *Current Pharmaceutical Biotechnology*, 19(1):5–18, 2018.

[34] H. Moore and N. K. Li. A mathematical model for chronic myelogenous leukemia (CML) and T cell interaction. *Journal of Theoretical Biology*, 227(4):513–523, Apr. 2004.

[35] N. Naveed, T. Gottron, J. Kunegis, and A. C. Alhadi. Bad news travel fast: a content-based analysis of interestingness on Twitter. In *Proceedings of the 3rd International Web Science Conference*, WebSci '11, pages 1–7, New York, NY, USA, June 2011. Association for Computing Machinery.

[36] K. Owens and I. Bozic. Modelling car t-cell therapy with patient preconditioning. *bioRxiv*, 2020.

[37] K. Owens and I. Bozic. Modeling CAR T-Cell Therapy with Patient Preconditioning. *Bulletin of Mathematical Biology*, 83(5):42, Mar. 2021.

[38] J. Peiró and S. Sherwin. Finite Difference, Finite Element and Finite Volume Methods for Partial Differential Equations. In S. Yip, editor, *Handbook of Materials Modeling: Methods*, pages 2415–2446. Springer Netherlands, Dordrecht, 2005.

[39] H. Rosenberg, S. Syed, and S. Rezaie. The Twitter pandemic: The critical role of Twitter in the dissemination of medical information and misinformation during the COVID-19 pandemic. *Canadian Journal of Emergency Medicine*, 22(4):418–421, July 2020. Publisher: Cambridge University Press.

[40] M. W. Scroggs, I. A. Baratta, C. N. Richardson, and G. N. Wells. Basix: a runtime finite element basis evaluation library. *Journal of Open Source Software*, 7(73):3982, 2022.

[41] M. W. Scroggs, J. S. Dokken, C. N. Richardson, and G. N. Wells. Construction of arbitrary order finite element degree-of-freedom maps on polygonal and polyhedral cell meshes. *ACM Transactions on Mathematical Software*, 2022. To appear.

[42] D. Sermer, C. Batlevi, M. L. Palomba, G. Shah, R. J. Lin, M.-A. Perales, M. Scordo, P. Dahi, M. Pennisi, A. Afuye, M. L. Silverberg, C. Ho, J. Flynn, S. Devlin, P. Caron, A. Hamilton, P. Hamlin, S. Horwitz, E. Joffe, A. Kumar, M. Matasar, A. Noy, C. Owens, A. Moskowitz, D. Straus, G. von Keudell, I. Rodriguez-Rivera, L. Falchi, A. Zelenetz, J. Yahalom, A. Younes, and C. Sauter. Outcomes in patients with DLBCL treated with commercial CAR T cells compared with alternate therapies. *Blood Advances*, 4(19):4669–4678, Oct. 2020.

[43] C. Shao, G. L. Ciampaglia, O. Varol, K. Yang, A. Flammini, and F. Menczer. The spread of low-credibility content by social bots. *Nature Communications*, 9(1):4787, Dec. 2018. arXiv:1707.07592 [physics].

[44] R. C. Sterner and R. M. Sterner. CAR-T cell therapy: current limitations and potential strategies. *Blood Cancer Journal*, 11(4):1–11, Apr. 2021. Number: 4 Publisher: Nature Publishing Group.

[45] K. R. Swanson, R. C. Rostomily, and E. C. Alvord. A mathematical modelling tool for predicting survival of individual patients following resection of glioblastoma: a proof of principle. *British Journal of Cancer*, 98(1):113–119, Jan. 2008.

[46] C. Tomasetti and D. Levy. An elementary approach to modeling drug resistance in cancer. *Mathematical biosciences and engineering: MBE*, 7(4):905–918, Oct. 2010.

[47] O. Tsur and A. Rappoport. What's in a hashtag? content based prediction of the spread of ideas in microblogging communities. In *Proceedings of the fifth ACM international conference on Web search and data mining*, WSDM '12, pages 643–652, New York, NY, USA, Feb. 2012. Association for Computing Machinery.

[48] L. Vogel. Viral misinformation threatens public health. *CMAJ*, 189(50):E1567–E1567, Dec. 2017. Publisher: CMAJ Section: News.

[49] M. Vogels, R. Zoeckler, D. M. Stasiw, and L. C. Cerny. P. F. Verhulst's "notice sur la loi que la populations suit dans son accroissement" from correspondence mathematique et physique. Ghent, vol. X, 1838. *Journal of Biological Physics*, 3(4):183–192, Dec. 1975.

[50] L. Weng, F. Menczer, and Y.-Y. Ahn. Virality Prediction and Community Structure in Social Networks. *Scientific Reports*, 3(1):2522, Aug. 2013. Number: 1 Publisher: Nature Publishing Group.

[51] K. C. Wong, R. M. Summers, E. Kebebew, and J. Yao. Tumor growth prediction with reaction-diffusion and hyperelastic biomechanical model by physiological data fusion. *Medical Image Analysis*, 25(1):72–85, 2015.

[52] T. Zaman, E. B. Fox, and E. T. Bradlow. A Bayesian approach for predicting the popularity of tweets. *The Annals of Applied Statistics*, 8(3), Sept. 2014. arXiv:1304.6777 [physics, stat].

[53] Q. Zhao, M. A. Erdogdu, H. Y. He, A. Rajaraman, and J. Leskovec. SEISMIC: A Self-Exciting Point Process Model for Predicting Tweet Popularity. In *Proceedings of the 21th ACM SIGKDD International Conference on Knowledge Discovery and Data Mining*, pages 1513–1522, Aug. 2015. arXiv:1506.02594 [physics, stat].

[54] K. B. Ølgaard and G. N. Wells. Optimisations for quadrature representations of finite element tensors through automated code generation. *ACM Transactions on Mathematical Software*, 37, 2010.